DOE-HTGR-88381
ORNL/TM-11455

HTGR

IMGA EXAMINATION OF SET #4 FUEL UNDER PROJECT WORK STATEMENT FD-20

AUTHORS/CONTRACTORS

Oak Ridge National Laboratory
C. A. Baldwin
M. J. Kania

Oak Ridge National Laboratory
Oak Ridge, Tennessee 37831-6285
operated by
MARTIN MARIETTA ENERGY SYSTEMS, INC.
for the
UNITED STATES DEPARTMENT OF ENERGY
March 1990

DOE-HTGR-88381
ORNL/TM-11455
Distribution
Category UC-522

Metals and Ceramics Division

IMGA EXAMINATION OF SET #4 FUEL UNDER PROJECT WORK STATEMENT FD-20

C. A. Baldwin
M. J. Kania

Date Published – March 1990

Prepared for the
U.S. Department of Energy
Office of Advanced Reactor Programs
AF 20 10 15 2

Prepared by the
OAK RIDGE NATIONAL LABORATORY
Oak Ridge, Tennessee 37831-6285
operated by
MARTIN MARIETTA ENERGY SYSTEMS, INC.
for the
U.S. DEPARTMENT OF ENERGY
under Contract DE-AC05-840R21400

CONTENTS

LIST OF TABLES

LIST OF FIGURES

IMGA EXAMINATION OF SET #4 FUEL UNDER PROJECT WORK STATEMENT FD-20*

C. A. Baldwin
M. J. Kania

ABSTRACT

Results of an examination of over 10,800 unbonded fuel particles from three irradiated spherical fuel elements by the Irradiated Microsphere Gamma Analyzer system are reported. The investigation was initiated to assess fission product behavior in LEU UO_2 TRISO-coated fuel particles at elevated temperatures. Of the three spheres considered, one was reserved as a control and the other two were subjected to simulated accident-condition temperatures of 1600°C and 1800°C, respectively. For the control sphere and the sphere tested at 1600°C, no statistical evidence of fission product release (cesium) from individual particles was observed. At fuel temperatures of 1800°C, however, fission product release (cesium) from individual particles was significant and there was large particle-to-particle variation. At 1800°C, individual particle release (cesium) was on average ten times the Kernforschungsanlage-measured integral spherical fuel element release value. Particle release data from the sphere tested at 1800°C indicate that there may be two distinct modes of failure at fuel temperatures of 1800°C and above.

1. INTRODUCTION

Unbonded coated particles from three irradiated spherical fuel elements from the Federal Republic of Germany (FRG) have been examined using the Irradiated Microsphere Gamma Analyzer (IMGA) system. The examinations were conducted under the U.S.-FRG Umbrella Agreement on High-Temperature Reactor (HTR) Development, Project Work Statement (PWS) FD-20. The particles are part of a shipment of irradiated fuel from FGR collectively known as Set #4 Fuels and represent the fourth series of such fuels to be examined at Oak Ridge National Laboratory (ORNL) under PWS FD-20. The purpose of the examinations are to provide detailed statistically significant data on failure fraction, quantification of fission product retention, and identification of released species. The examination method of primary interest is the IMGA system, and together with analytic tools developed at ORNL, it represents a unique system for characterizing the

*Research sponsored by the Office of Advanced Reactor Programs, Division of HTGRs, U.S. Department of Energy, under contract DE-AC05-84OR21400 with Martin Marietta Energy Systems, Inc.

performance of a large population of high-temperature gas-cooled reactor (HTGR) coated-particle fuels with statistical significance.

2. DESCRIPTION OF FRG SET #4 FUELS

A portion of the unbonded particles from three irradiated spherical fuel elements have been examined by the IMGA system. The parent spheres from which the unbonded particles were obtained are identified as AVR-76/20, HFR-K3/1, and HFR-K3/3. The coated particles in all three spheres were FRG reference LEU UO_2 TRISO-coated particles, and they, along with the spherical fuel elements, were fabricated to HTR-module quality specifications by the FRG HTR fuel manufacturer HOBEG, GmbH.

2.1 IRRADIATION HISTORY

Sphere AVR-76/20 was irradiated in the Arbeitsgemeinschaft Versuchsreaktor (AVR) located at Jülich, FRG, and was part of reload #19, which was initially loaded into the reactor in 1982. The UO_2 fuel kernels were originally 10% enriched, and at discharge from the AVR, the sphere had achieved a burnup of 6.5% fissions per initial heavy-metal atom (FIMA). The AVR is a pebble bed HTR, and the irradiation was real-time, so temperature monitoring of the fuel sphere was not possible. Thus, irradiation temperatures can only be estimated. Estimates for the irradiation temperature of sphere AVR-76/20 were in the range of 800°C to 1000°C. The accumulated fast neutron fluence received by this sphere was very low, estimated at less than 1.8×10^{25} neutrons/m^2. The irradiation data for sphere AVR-76/20 is summarized in Table 1.

Table 1. Irradiation history of Set #4 fuels from PWS FD-20

Sphere	Operating temperature (°C)	Burnup (% FIMA)	Accumulated fluence[a]
AVR-76/20	800 - 1000	6.5	<1.8E+25
HFR-K3/1	1000 - 1200	7.7	3.9E+25
HFR-K3/3	800 - 1000	10.2	6.0E+25

[a]Fluence values are in units of neutrons/m^2, $E \geq 0.1$ MeV.

The two spheres from experiment HFR-K3 were irradiated in the High Flux Reactor (HFR) located at Petten, Netherlands. The experimental assembly of HFR-K3, specifically designed for HTR spherical fuel element testing, contains three separate capsules, each with an independent sweep gas system and temperature control. The UO_2 fuel kernels from which the HFR-K3 elements were fabricated came from batch EO-2308 and were initially

enriched to 9.82%. After 359 full power days in the HFR, the experiment was discharged from the reactor, the irradiation rig disassembled, and the major components shipped to Kernforschungsanlage (KFA), in Jülich, FRG, for postirradiation examination. Sphere HFR-K3/1 was irradiated in the uppermost capsule at an operating temperature ranging from 1000°C to 1200°C. It accumulated a fast neutron fluence of 3.9×10^{25} neutrons/m^2. The irradiation temperature for sphere HFR-K3/3, located in the middle capsule of the test rig, was 800°C to 1000°C, and the fluence received was 6.0×10^{25} neutrons/m^2. Burnups for the two spheres, HFR-K3/1 and HFR-K3/3, were determined to be 7.7% FIMA and 10.2% FIMA, respectively. The operating data during irradiation of spheres HFR-K3/1 and HFR-K3/3 are summarized in Table 1.

2.2 CORE HEATUP SIMULATION TESTING

Following irradiation, the two HFR-K3 spheres were subjected to core heatup simulation tests in a specially designed high-temperature facility located in the hot cells at KFA-Jülich.[1] Sphere HFR-K3/1 was subjected to a 500-h isothermal test at 1600°C. During this test, the fission products released from the sphere were collected and analyzed. The gaseous species were collected in activated charcoal cold traps, and the metallic species were collected on a deposition surface placed within the high-temperature furnace. This surface can be removed and replaced through a gate-valve system allowing the furnace to maintain temperature during the operation. Sphere HFR-K3/3 was isothermally heated for two periods at 1800°C: for a 25-h period and then for a 75-h period. During both heating periods, fission product release was carefully monitored and analyzed. The sphere AVR-76/20 was not subjected to postirradiation heating.

The time-dependent release of ^{85}Kr and the condensable radioisotopes ^{90}Sr, ^{110m}Ag, and ^{137}Cs are shown in Fig. 1 for the two HFR-K3 spheres. The 200°C-higher test temperature for sphere HFR-K3/3 had a significant effect on the rate of release of all the radioisotopes. A comparison of the cesium release fraction at similar temperatures during the heatup phase of each simulation test is given in Table 2. These data indicate that the cesium release characteristics of the two spheres were quite similar at the start of the accident-simulation testing; however, by the time sphere HFR-K3/3 had reached 1800°C, the ^{137}Cs release fraction had increased to 3.6×10^{-6} and was rapidly increasing. After 25-h at 1800°C, sphere HFR-K3/3 exhibited a cesium release fraction of 1.0×10^{-3}, and the rate was increasing; whereas after 75-h at 1600°C, the cesium release fraction for sphere HFR-K3/1 was about 2.2×10^{-6} and maintaining a relatively stable release. Only after more than 200-h at 1600°C did the slope of the cesium release curve for sphere HFR-K3/1 begin to increase at a rapid rate. The integral radioisotope release data at the end of each accident-simulation test is shown in Table 3. Sphere HFR-K3/3 released an average of 6.2% of its total cesium at the end of 100-h at 1800°C, compared to about 0.012% for sphere HFR-K3/1 after 500-h at 1600°C.

ORNL-DWG-90-8079

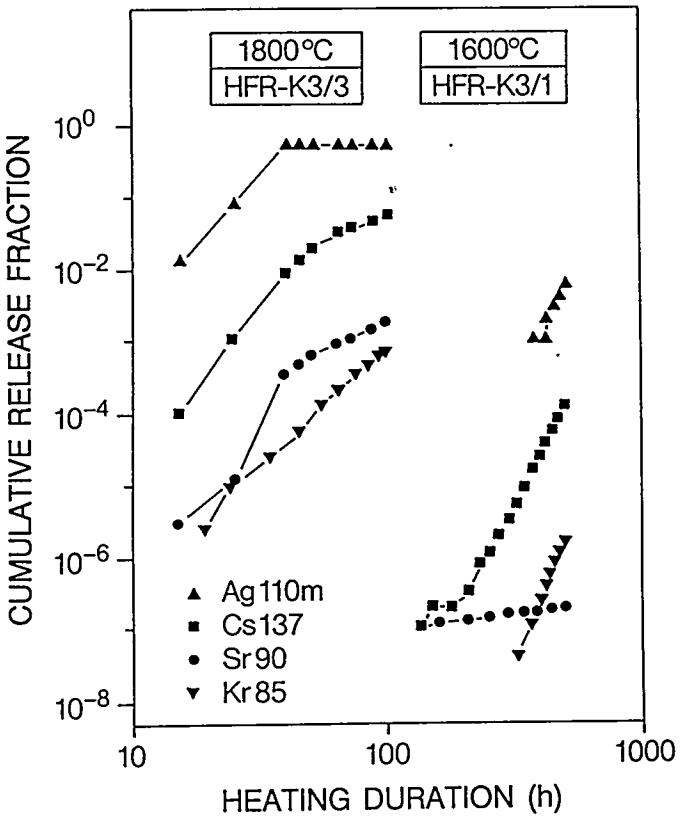

Fig. 1. Time-dependent release during accident-simulation tests for spheres HFR-K3/1 and HFR-K3/3.

Table 2. Cesium release fraction at similar temperatures for spheres HFR-K3/1 and HFR-K3/3

Temperature (°C)	^{137}Cs release fraction	
	HFR-K3/1	HFR-K3/3
1250	3.12E-07	2.5E-07
1500	4.13E-07	-
1550	-	4.9E-07
1600	6.45E-07	-
1800	-	3.6E-06

Table 3. Integral radioisotope release results measured during KFA accident-simulation tests

Isotope	Integral fractional release	
	HFR-K3/1	HFR-K3/3
^{85}Kr	1.8E-06	6.5E-04
^{90}Sr	8.3E-06	1.8E-03
^{110m}Ag	2.7E-02	6.7E-01
^{134}Cs	1.3E-04	6.4E-02
^{137}Cs	1.1E-04	5.9E-02

2.3 FUEL SPHERE DECONSOLIDATION PROCEDURE

Unbonded particles from the three spheres were obtained by utilizing a two-part electrolytic deconsolidation process employed at KFA and illustrated in Fig. 2. The first part of the deconsolidation process removes the outer circumference of the sphere and leaves a cylinder approximately 2 cm in diameter. In the second part of the process, the remaining cylinder is rotated 90° and lowered into the electrolyte in 10 discrete steps. After each step is deconsolidated, the unbonded particles are collected and packaged separately. Thus, for each sphere, 11 samples of unbonded particles are obtained, with 10 of the samples providing a profile of fuel from the edge to the center of the sphere.

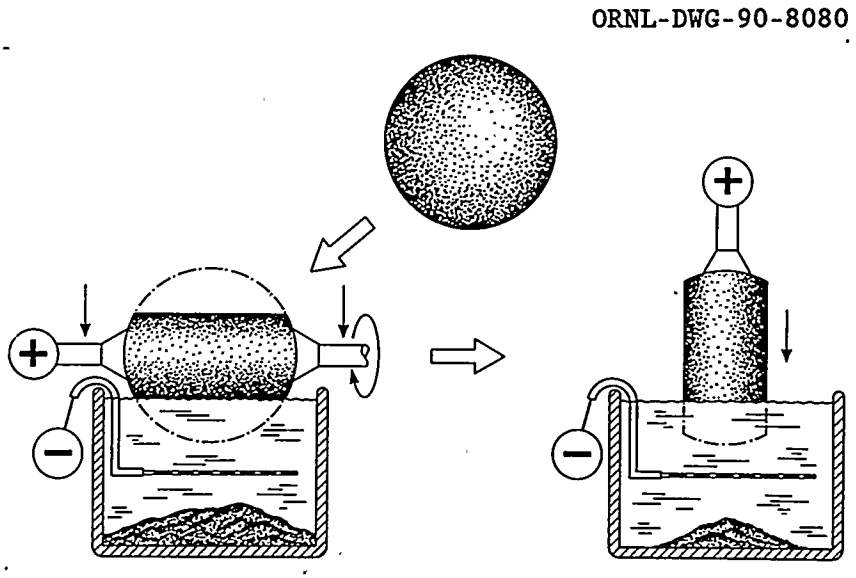

Fig. 2. Spherical fuel element deconsolidation procedure employed at KFA.

2.4 FUEL PARTICLE DESCRIPTION

TRISO-coated particles from batch EO-2308 employ a UO_2 fissile kernel surrounded by a buffer layer of low-density carbon, an inner pyrocarbon layer, a silicon carbide layer, and finally an outer pyrocarbon layer. The parameters given in Table 4 are nominal values for the batch.

Table 4. Nominal design parameters for particles in batch EO-2308

Description	Size	Density (Mg/m^3)
Kernel: UO_2 (10% enriched)	497 μm diam	10.81
TRISO coating: Buffer	94 μm thick	1.00
IPyC	41 μm thick	1.88
SiC	36 μm thick	3.20
OPyC	40 μm thick	1.88

During initial test examinations of fuel from Set #4, a problem was encountered. The design of the IMGA particle handler will allow only those particles with a diameter less than 1250 μm to be safely transported. The nominal diameter of the TRISO-coated particles from these three spheres is about 920 μm; however, some of the particles retained the porous carbon overcoating, which increases the diameter to about 1320 μm. Normally the overcoating is removed during the electrolytic deconsolidation process, but in the two HFR-K3 spheres a significant fraction of the particles retained their overcoatings. It is not known if the postirradiation core heatup simulation testing caused the problem or whether there was some abnormality in the deconsolidation process itself. In any event, it was necessary to remove the overcoated particles before the samples could be examined by IMGA. This was accomplished by using several wire sieves to grade the unbonded particles by size. It was observed that about 1% of the AVR-76/20 particles, 30% of the HFR-K3/1 particles, and 50% of the HFR-K3/3 particles retained their overcoatings. These particles have been set aside, and only the clean particles that were separated out have been examined. Representative photographs made during the initial visual examination of the particles are shown in Fig. 3.

3. THE IRRADIATED MICROSPHERE GAMMA ANALYZER

The IMGA system is a unique research tool located in the High Level Radiation Examination Laboratory (HRLEL) at ORNL. The primary function of the IMGA system is to measure accurately radioisotopic inventories of individual coated particles used in HTGR applications. This is accomplished by detecting the gamma radiation given off by the fuel particles as various fission/activation products decay. The system consists of

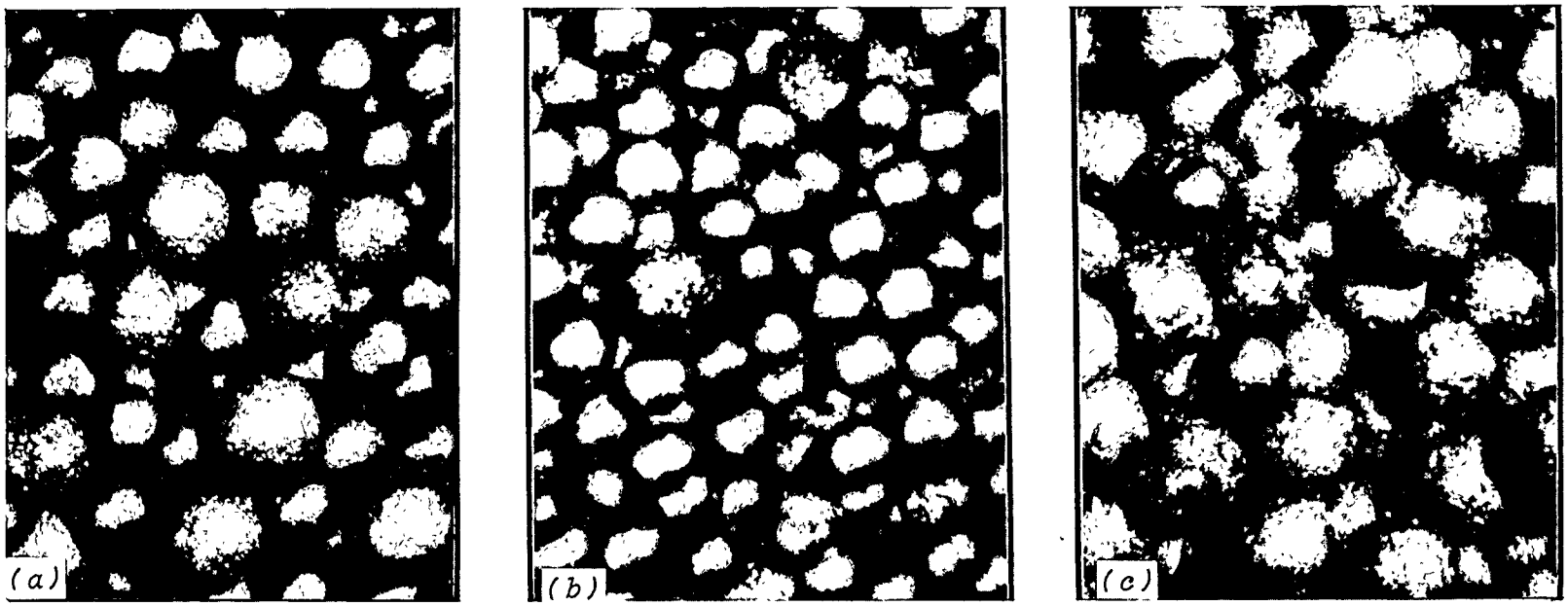

Fig. 3. Representative photographs showing mixture of clean and overcoated particles as received from FRG: (a) sphere AVR-76/20, step 5; (b) sphere HFR-K3/1, step 10; and (c) sphere HFR-K3/3, step 5.

three major components: (1) a high-resolution gamma-ray spectrometer, (2) a computer-based multichannel analyzer, and (3) an automated particle-handling system. The three components have been integrated into a sophisticated system capable of autonomous operation.

3.1 IMGA COMPONENTS

The IMGA system utilizes an ORTEC GMX Series GAMMA-X HPGe (high-purity germanium) coaxial photon spectrometer for radiation detection. The spectrometer has a 0.5-mm-thick beryllium window and is operated at a bias of −3000 V. Output from the spectrometer's internal preamplifier is first routed through an ORTEC Model 572 amplifier and then into a Nuclear Data ND581 analog-to-digital converter (ADC). The ND581 is a high-speed, high-resolution ADC, capable of digitizing 160,000 events/s with a fixed conversion time of 5 μs. This configuration has been adjusted to yield gamma-ray spectral data from approximately 3 keV to 2 MeV.

The multichannel analyzer (MCA) used by the IMGA system is a Nuclear Data ND6700 Data Acquisition and Processing System. The ND6700 consists of a computer system tightly coupled to an MCA with both computer and analyzer sharing portions of the computer memory. The central processing unit is a Digital Equipment Corporation (DEC) LSI-11 microcomputer with extended and floating-point instruction sets utilized in a non-DEC environment. The ND6700 uses a multiprocessor and multiuser operating system, MIDAS/M, which can accommodate up to four processors and execute up to four tasks in parallel.

The automated particle handler shown in Fig. 4 is the unique component in the IMGA system. It is composed of three main parts – a singularizer, a sample changer, and a sample collector – which are all synchronized and controlled by the ND6700 computer. The singularizer isolates an individual microsphere from a given sample and transfers it to the sample changer. The sample changer moves the microsphere from the loading position below the singularizer to the counting position in front of the spectrometer. After the microsphere is counted, the sample changer moves the particle to the unloading position above the sample collector. The sample collector has 20 bin locations that can be used to segregate fuel into different categories. The handler is located in a shielded cubicle on the second floor of the HRLEL directly above the main hot cells on the first floor. A transfer device allows irradiated fuel to be moved in and out of the cubicle from the hot cells below without having to breach alpha containment.

3.2 IMGA OPERATION

Operation of the IMGA system is controlled entirely by the ND6700 computer system. Initially, a setup program positions all parts of the particle-handling system, allocates MCA ports and memory, acquires and stores a background spectrum, and begins searching for an active particle.

In the singularizer, particles are loaded onto an inclined chute that terminates at a drum assembly. The drum has two very small diameter holes

YP-9976

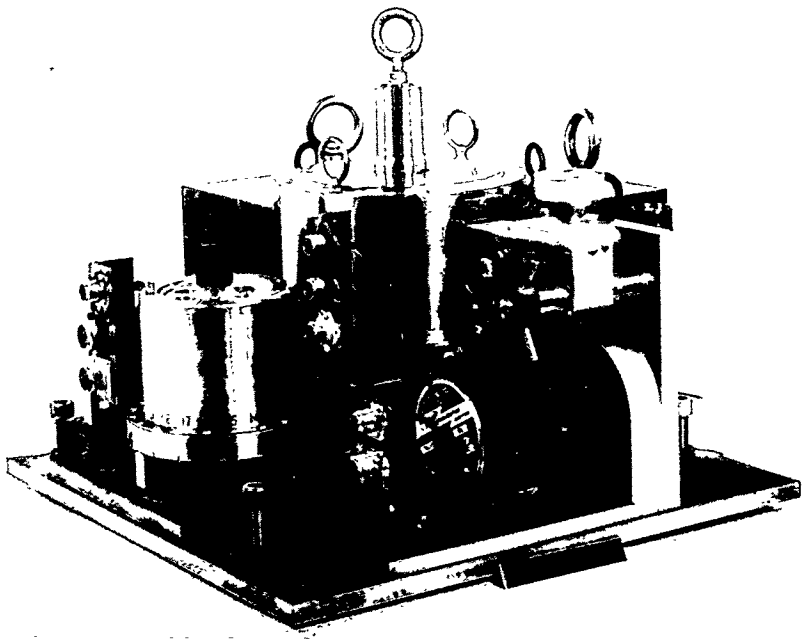

YP-9975

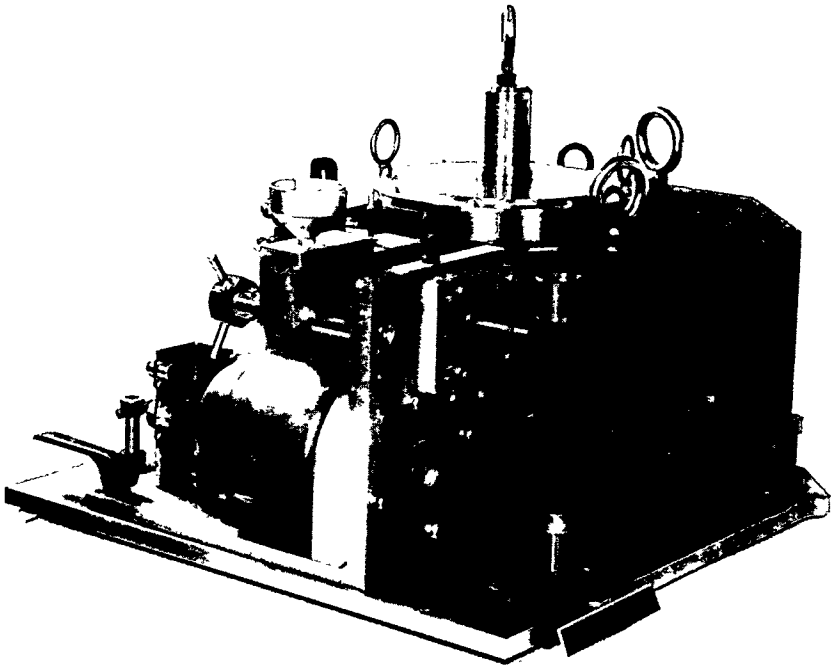

Fig. 4. Two views of the IMGA automated particle handler shown before installation in the shielded IMGA cubicle.

drilled 180° apart that line up with the apex of the chute. The drum interior is held at low pressure by a vacuum pump such that suction is always applied at the small holes. The drum is rotated on demand by the computer, and as it passes by the particles located on the inclined chute, it picks up a single particle. If a particle is attached to the opposite hole, 180° from the particle just loaded, it is simultaneously dropped into the sample changer assembly. This is accomplished by means of a reciprocating pin mechanically linked inside the drum which alternately opens the hole on the chute side and closes the hole on the opposite side.

As the particles are released from the singularizer they are guided into one of four holders in the sample changer assembly and are rotated counterclockwise 90° into position in front of the spectrometer. The computer then initiates acquisition through the MCA, and a gamma-ray energy spectrum is acquired. After acquisition is terminated, the particle is again rotated 90° counterclockwise to a holding position where a quantitative analysis is performed on the gamma-ray energy spectrum. The first active particle identified by the system is treated differently from later particles. This first gamma-ray spectrum is acquired and saved in a disk file, the background is stripped away, a peak search and nuclide identification analysis are performed, and then the program enters a selection mode where the operator interactively picks out photopeaks of interest. The channels associated with the selected peaks are stored in memory so that in the energy spectrum analysis of future particles, it is necessary to analyze only those portions selected during setup. After completing these particle-handler setup procedures, no further operator intervention is necessary. Subsequent particles are then isolated automatically and positioned in front of the spectrometer for counting. Gamma spectra are acquired and analyzed, and the results are recorded in a disk file for later detailed analysis.

The final function of the particle handler is to classify each particle. The sample changer is rotated once again 90° counterclockwise (third rotation) to a position above the unloading assembly. A special user-programmed subroutine is called before each particle is unloaded from the sample changer into the collector assembly. The collector contains a total of 20 bins in which the particles can be partitioned. Bin-selection criteria are based on the measured photopeak intensities and make it possible to physically separate particles as a function of their ability to retain key radioisotopes.

4. IMGA EXAMINATION RESULTS

All unbonded particles free of overcoatings from the central cylinders of the three spheres have been examined. Table A.1 in Appendix A provides a stepwise summary of the number of individual particle records obtained from each deconsolidation step and the starting date for the examination run. Particle records where two or more particles were counted simultaneously have been eliminated from the analysis. Fortunately, these multiple loads account for less than 0.5% of the total number of examination records. Two particle records, one each from

spheres AVR-76/20 and HFR-K3/1, were omitted from the overall analysis because of the uncharacteristic nature of their data. Their activities and activity ratios appear separately in Tables A.3, A.4, A.18, and A.19. The particle from the AVR-76/20 sphere appears to have an unusually large kernel, and the particle from the HFR-K3/1 sphere has low inventories of all isotopes measured. These two anomalous particles have been isolated and are available for additional tests.

Each particle was counted for a spectrometer live-time of 240 s. Photopeak counting errors were in the ±1.5% to ±5.0% range (1σ) for the isotopes ^{106}Ru, ^{144}Ce, and ^{154}Eu and better than ±1% (1σ) for the isotopes ^{134}Cs and ^{137}Cs. For comparison purposes it was necessary to convert the photopeak count rates to activities at the end of irradiation. Parameters used to calculate absolute activities from the count rates measured by IMGA are given in Table A.2 for the fission/activation products of interest. The detector efficiencies in this table are unique to the IMGA spectrometer and counting geometry and were obtained by careful calibration against both National Institute of Standards and Technology (formerly National Bureau of Standards) and Amersham calibration sources. The decay constants and branching ratios in the table were taken from Kocher.[2] The self-shielding correction factors for each photon energy were calculated by an interactive computer program, SSCF, under development at ORNL. The self-shielding calculation was based on the particle description and burnups given in Sect. 2.

Tables A.3 through A.5 in Appendix A are stepwise summaries of mean fission/activation product activities and associated standard deviations for ^{106}Ru, ^{134}Cs, ^{137}Cs, ^{144}Ce, and ^{154}Eu for the three spheres. As the data in these tables make evident, the distribution of fission/activation products in a fuel sphere is not uniform and in fact can vary considerably. For chemically stable isotopes like ^{106}Ru and ^{144}Ce the variation is probably due to differences in production rates, which are directly related to fuel burnup. This is illustrated most clearly in Table A.4, which gives data for the HFR-K3/1 sphere. Unlike the other two spheres, sphere HFR-K3/1 was irradiated in an experimental position where a significant thermal flux gradient existed from the top to the bottom of the sphere. The expected surface-to-center burnup gradient due to thermal neutron self-shielding has been skewed to one side, and a 13.1% difference exists between the maximum and minimum mean values for the ^{144}Ce activity. For the AVR-76/20 sphere, the difference between maximum and minimum mean values for the ^{144}Ce activity is only 3.8%, and the gradient from surface to center is almost symmetric. For the more volatile isotopes like ^{134}Cs, ^{137}Cs, and ^{154}Eu, the distributions are probably due to a combination of both production and release mechanisms.

In determining particle failure it is accepted practice to normalize the product activity of interest to a nonvolatile product activity to account for the variable masses of the individual particles. A particle that exhibits an unusually low value for a given ratio would be suspected of failing to retain the isotope in question. Because of the lengthy delay between the end of irradiation and the examination of the particles by IMGA, choices for a suitable reference isotope were limited to ^{106}Ru and ^{144}Ce. The latter isotope, ^{144}Ce, proved to be the best reference isotope for the fuels examined from Set #4 because of its stability in oxide fuels

and its superior counting statistics. Tables A.6 through A.17 in Appendix A summarize the distribution of ^{106}Ru:^{144}Ce, ^{134}Cs:^{144}Ce, ^{137}Cs:^{144}Ce, and ^{154}Eu:^{144}Ce ratios for the spheres AVR-76/20, HFR-K3/1, and HFR-K3/3, respectively. In these tables, occurrences of a given ratio are tabulated in histogram channels that were set up by dividing the total range (maximum ratio to minimum ratio) for a given sphere into 25 discrete channels. At this point all that can be stated is that the distributions for the AVR-76/20 sphere are "normal like" and characteristic of no particle failures. The distributions for the HFR-K3/1 sphere are broader than the corresponding AVR-76/20 distributions and are somewhat asymmetric; however, the broadening and asymmetry appear to be caused by uneven burnup and are not necessarily due to particle failure. The "bimodal" distributions observed in the HFR-K3/3 sphere for the ^{134}Cs:^{144}Ce and ^{137}Cs:^{144}Ce ratios are indicative of particle failure, and there appear to be significant numbers of failed particles. It was found that particles near the surface of sphere HFR-K3/3 lost proportionally more cesium on average than particles near the center of the sphere. In contrast, the ^{154}Eu:^{144}Ce ratios for sphere HFR-K3/3 seem to indicate a major "normal like" distribution of particles that have retained their europium, with only a few particles in the center region of the sphere showing europium loss. Tables A.18 through A.20 are stepwise summaries of the mean activity ratios and associated standard deviations for each of the three spheres and are provided for reference purposes.

5. FISSION PRODUCT RETENTION ANALYSIS

In order to determine how much of a given fission or activation product a particle has retained, it is necessary to know the inventory that should be present in the particle assuming nothing has escaped. Normally such information requires detailed calculations of the buildup, decay, and burnup of individual isotopes during the irradiation period and subsequent out-of-reactor hold-time for the fuel. Unfortunately, for the three fuel elements of interest here, such detailed calculations were not available. As an approximation, the assumption is made that no loss of fission or activation products occurred from the parent fuel elements during their irradiation. For the two HFR-K3 elements, this assumption can be verified by looking at their end-of-life (EOL) fission gas release rate vs birth rate (R/B) values. Capsules 1 and 2 of experiment HFR-K3 contained spheres 1 and 3, respectively. The capsule beginning-of-life (BOL) and EOL ^{85m}Kr R/B values are given in Table 5. The EOL values indicate that for both spheres the EOL ^{85m}Kr R/B is less than 2×10^{-7}. Using a gas release value for a failed UO_2 particle $[(R/B)_f]$ of about 2×10^{-2}, the EOL capsule R/B data represents a $\leq 1 \times 10^{-5}$ failed particle fraction. Approximately 32,800 particles were contained in the two spheres in each capsule, so this activity represents <33% of a single particle inventory. Therefore, the activity must be due to the heavy metal contaminations present in the sphere from fabrication. The low EOL R/B data is representative of no failed UO_2 particles in either HFR-K3/1 or HFR-K3/3 based on gas-release data. Data on EOL R/B were not available for sphere AVR-76/20 to perform a similar analysis.

Table 5. Experiment HFR-K3 BOL and EOL ^{85m}Kr R/B values

Experiment and capsule	^{85m}Kr R/B	
	BOL	EOL
HFR-K3/Capsule 1	1.3E-09	<2E-07
HFR-K3/Capsule 2	8.0E-10	<2E-07

Coupled measurements and calculations performed at KFA-Jülich on each fuel sphere at the end of irradiation were used to estimate particle average activities. The sphere total activities reported by KFA were divided by 16,400 particles per sphere to determine the particle average activities. The particle average activities for IMGA were obtained by combining the total population of particles from each sphere into a single data set and computing the means and standard deviations for the activities derived from each photopeak. Where multiple photopeaks for a given isotope were analyzed, an arithmetic mean was used to represent the particle average activity for the sphere. Tables 6 through 8 give the comparisons between IMGA and KFA fission/activation product activities for the spheres AVR-76/20, HFR-K3/1, and HFR-K3/3, respectively. The last column in each table gives the ratio of the IMGA particle average activity to the KFA particle average activity. Note that for the two HFR-K3 spheres two sets of data from KFA were reported and in most instances were in close agreement. The exception was the activity for ^{144}Ce, which was approximately 15% lower in ref. 1. The reason for the discrepancy between the two KFA values is not known; the higher values were used here because

Table 6. Comparison of ORNL and KFA activities for sphere AVR-76/20

Isotope	ORNL[a]				KFA[b]		ORNL/KFA
	Photon (KeV)	Mean[c]	s (%)	Particle[c] average	Sphere total	Particle[c] average	
^{106}Ru	511	1.15E+07	4.9	1.13E+07	1.80E+11	1.10E+07	1.03
	622	1.11E+07	5.3				
^{134}Cs	604	2.73E+06	2.9	2.76E+06	4.90E+10	2.99E+06	0.92
	795	2.78E+06	2.9				
^{137}Cs	662	3.71E+06	2.5	3.71E+06	7.30E+10	4.45E+06	0.83
^{144}Ce	133	4.62E+07	2.8	4.62E+07	7.20E+11	4.39E+07	1.05
^{154}Eu	1274	7.42E+04	8.0	7.42E+04	1.41E+09	8.60E+04	0.86

[a]Results based on analysis of 4940 particles from steps 1 to 10.

[b]Data taken from ref. 1, table 51.

[c]Bq per particle on October 17, 1985.

Table 7. Comparison of ORNL and KFA activities for sphere HFR-K3/1

Isotope	ORNL[a]				KFA[b]		ORNL/KFA
	Photon (KeV)	Mean[c]	s (%)	Particle[c] average	Sphere total	Particle[c] average	
^{106}Ru	511	2.34E+07	10.6	2.29E+07	3.66E+11	2.23E+07	1.03
	622	2.23E+07	11.3				
^{134}Cs	604	5.31E+06	11.3	5.31E+06	9.26E+10	5.65E+06	0.94
	795	5.40E+06	11.4				
	1364	5.22E+06	12.7				
^{137}Cs	662	4.73E+06	6.5	4.73E+06	8.88E+10	5.41E+06	0.87
^{144}Ce	133	8.90E+07	6.2	8.90E+07	1.52E+12[d]	9.27E+07	0.96
^{154}Eu	123	1.62E+05	12.5	1.55E+05	2.86E+09	1.74E+05	0.89
	723	1.53E+05	14.1				
	1005	1.55E+05	13.7				
	1274	1.50E+05	12.0				

[a]Results based on analysis of 3514 particles from steps 1 to 10.
[b]Data taken from ref. 1, table 51.
[c]Bq per particle on September 5, 1983.
[d]Cerium data taken from ref. 3, sect. 3.3.2.2, table 1a.

Table 8. Comparison of ORNL and KFA activities for sphere HFR-K3/3

Isotope	ORNL[a]				KFA[b]		ORNL/KFA
	Photon (KeV)	Mean[c]	s(%)	Particle[c] average	Sphere total	Particle[c] average	
^{106}Ru	511	3.94E+07	7.0	3.88E+07	6.18E+11	3.77E+07	1.03
	622	3.81E+07	7.8				
^{134}Cs	604	4.78E+06	46.4	4.83E+06	1.82E+11	1.11E+07	0.43
	795	4.86E+06	46.9				
	801	4.85E+06	47.0				
	1364	4.82E+06	46.4				
^{137}Cs	662	3.00E+06	46.9	3.00E+06	1.19E+11	7.26E+06	0.41
^{144}Ce	133	1.17E+08	4.9	1.17E+08	1.91E+12[d]	1.16E+08	1.01
^{154}Eu	123	2.95E+05	7.8	2.85E+05	5.24E+09	3.20E+05	0.89
	723	2.83E+05	9.5				
	1005	2.83E+05	9.2				
	1274	2.77E+05	7.9				

[a]Results based on analysis of 2388 particles from steps 1 to 10.
[b]Data taken from ref. 1, table 51.
[c]Bq per particle on September 5, 1983.
[d]Cerium data taken from ref. 3, sect. 3.3.2.2, table 3a.

of their good agreement with IMGA measurements. Cerium in oxide kernels is known to form stable compounds even at high temperatures. Because of this, the cerium inventories measured with IMGA are the most representative of the actual particle inventory, as they represent direct measurements performed on several thousand particles.

The good agreement between IMGA and KFA pre-heatup simulation test data for the nonvolatile isotopes ^{106}Ru and ^{144}Ce for all three spheres implies no loss of these two isotopes from the individual fuel particles. For the ^{134}Cs, ^{137}Cs, and ^{154}Eu isotopes, however, the IMGA values are consistently lower than KFA pre-heatup data. This is to be expected for the two HFR-K3 spheres which were subjected to core heatup simulation tests; unfortunately, a mass balance of integral release data derived from condensate plates and the analysis of matrix graphite is not sufficient to account for the differences observed between the IMGA and KFA release data. Table 9 summarizes the integral release data for the condensate

Table 9. Fraction of cesium released to matrix graphite and condensate plates for spheres AVR-76/20, HFR-K3/1, and HFR-K3/3

Sphere	Isotope	Harwell[a]		KFA[b]	
		Matrix graphite	Condensate plate	Matrix graphite	Condensate plate
AVR-76/20	^{134}Cs	1.1E-05	-	-	-
	^{137}Cs	6.3E-06	-	-	-
HFR-K3/S1	^{134}Cs	1.6E-03	1.4E-04	-	1.3E-04
	^{137}Cs	1.8E-03	1.2E-04	1.2E-03	1.1E-04
HFR-K3/S3	^{134}Cs	8.7E-02	1.2E-01	-	6.4E-02
	^{137}Cs	9.7E-02	1.3E-01	8.2E-02	5.9E-02

[a]Data taken from ref. 4, tables 25 and 26.
[b]Data taken from ref. 1, tables 61, 97, and 139.

plates and the matrix graphite as reported by KFA and Harwell Laboratories for the two cesium isotopes. Similar data for the ^{154}Eu isotope were not available. Cesium not detected leaving the spheres (via condensate plates) and not held in the matrix graphite should be retained in the individual fuel particles. From Table 9 it is apparent that a negligible amount of cesium was released from the fuel particles in the AVR-76/20 sphere. For the HFR-K3/1 sphere, less than 0.2% of the cesium was released, and for the HFR-K3/3 sphere less than 23% of the cesium was released. These inventories are insufficient to explain the cesium releases implied by the ratios in Tables 6 through 8, of approximately 12%, 10%, and 58% for the spheres AVR-76/20, HFR-K3/1, and HFR-K3/3, respectively.

Part of the discrepancy may be due to the fact that the sample of particles examined by IMGA is not truly representative of the sphere as a whole. A disproportionate number of particles in the IMGA analysis came from the interior of the sphere. Since many more particles are located near the outer circumference, the mean IMGA-measured activities are biased to those activities consistent with the central portion of each sphere. Although a detailed analysis of the sampling method has not been undertaken in this report, it is unlikely that a sampling bias alone will resolve the 35% difference between the IMGA and KFA data for sphere HFR-K3/3. In fact, the stepwise data for sphere HFR-K3/3 indicate that particles exhibiting greater cesium loss have been undersampled.

To compare fission/activation product behavior directly between the three spheres, fission/activation product ratios were analyzed with a common set of histogram boundaries. The boundaries were determined by selecting the largest and smallest values for a given ratio from all three spheres and dividing the resulting range into 40 channels. The distributions, in histogram form, are presented graphically in Figs. 5 through 8. In the figures, the square root of the particle frequency was plotted to show more explicitly channels that contain only a few particles.

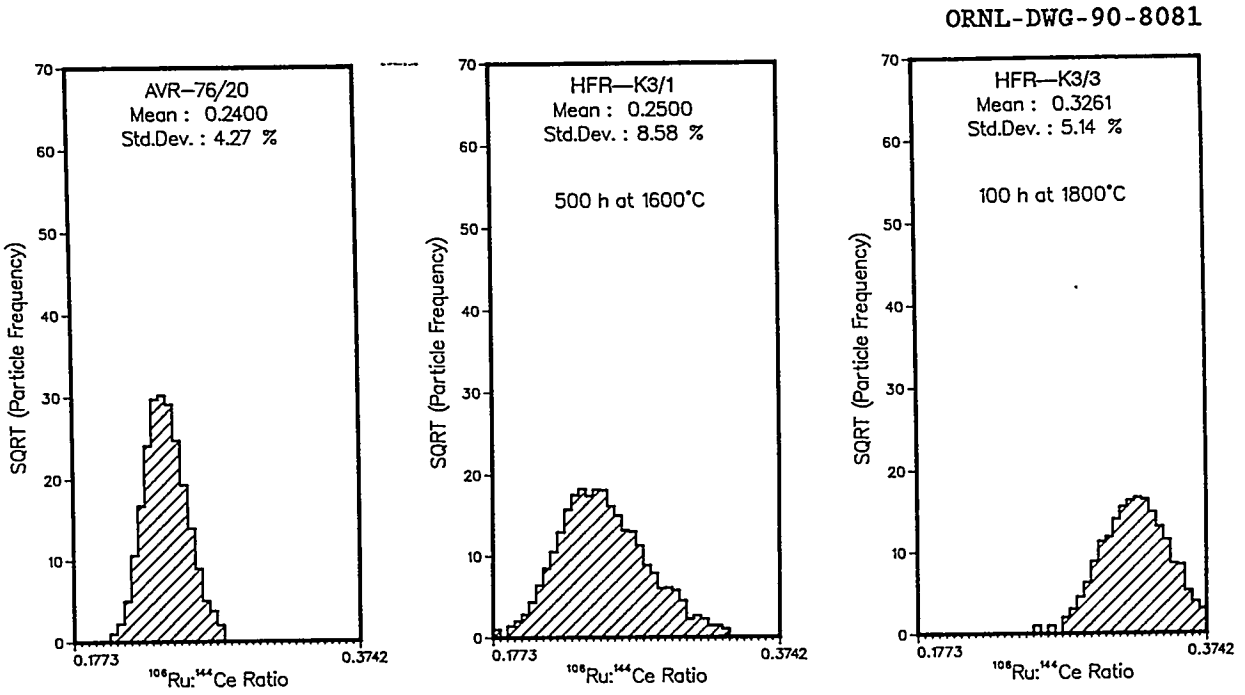

Fig. 5. Comparison of $^{106}Ru:^{144}Ce$ ratio distributions for spheres AVR-76/20, HFR-K3/1, and HFR-K3/3.

ORNL-DWG-90-8082

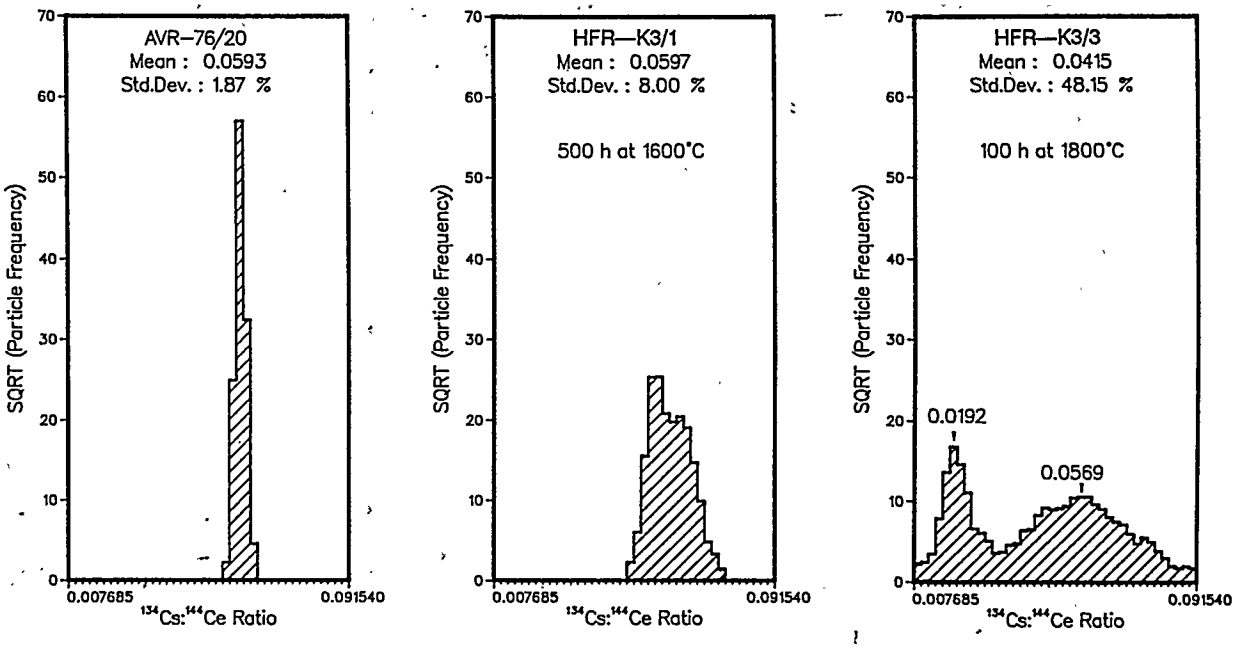

Fig. 6. Comparison of $^{134}Cs:^{144}Ce$ ratio distributions for spheres AVR-76/20, HFR-K3/1, and HFR-K3/3.

ORNL-DWG-90-8083

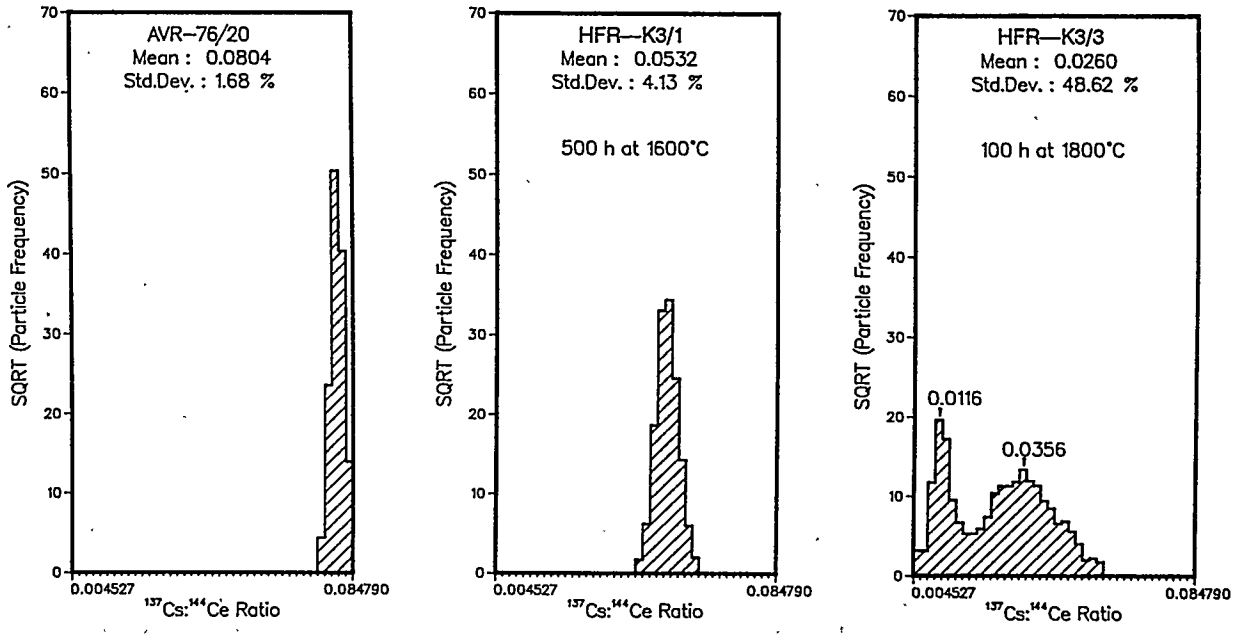

Fig. 7. Comparison of $^{137}Cs:^{144}Ce$ ratio distributions for spheres AVR-76/20, HFR-K3/1, and HFR-K3/3.

ORNL-DWG-90-8084

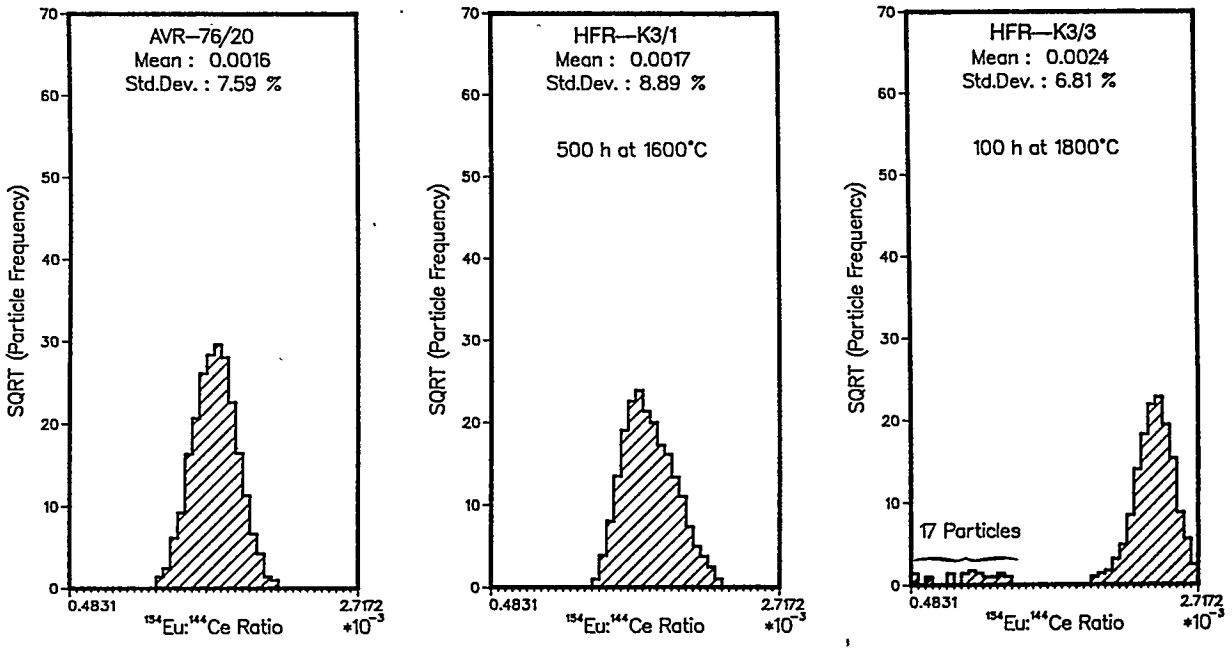

Fig. 8. Comparison of $^{154}Eu:^{144}Ce$ ratio distributions for spheres AVR-76/20, HFR-K3/1, and HFR-K3/3.

Figure 5 shows three histograms that illustrate the distribution of $^{106}Ru:^{144}Ce$ ratios for the three spheres. The AVR–76/20 and HFR–K3/3 particle data have "normal like" distributions and similar standard deviations, while the HFR–K3/1 particle data appear to be distributed somewhat more asymmetrically and cover a broader range of values. The asymmetry and broadening of the HFR–K3/1 particle data are thought to be caused by irregular burnup of the fuel due to the sphere's position in the HFR–K3 irradiation capsule and not caused by particle failure. This conclusion was reached because there are no particles that exhibit abnormally low ratios on the left side of the major distribution. In actuality, all three of these distributions fail to reveal any particles with abnormally low ratios. This fact along with the good absolute agreement with KFA pre-heatup data for ^{106}Ru and ^{144}Ce supports the assertion that all of the particles examined thus far have retained their ruthenium and cerium inventories.

Figures 6 and 7 show the histograms for the $^{134}Cs:^{144}Ce$ and $^{137}Cs:^{144}Ce$ distributions for the three spheres. In terms of fission/activation product retention, the behavior of the two cesium isotopes was the same; thus, the following discussion applies to both. The histogram for the AVR-76/20 sphere has a limited number of degrees of freedom owing to the selection of histogram boundaries; however, it appears "normal like," and there are no particles with unusually low ratios. This finding contradicts to some extent the previous comparison of IMGA and KFA pre-heatup data, which indicated cesium losses on the order of 12%. The only way for these two findings to be reconciled is for each individual particle to have lost

≈12% of its cesium inventory, which seems unlikely. A cesium loss of this mag-nitude would surely have shown up in the analysis of the matrix graphite. A more reasonable hypothesis is that there is a normalization bias between the IMGA and KFA data for cesium and that there were in fact no failed particles detected in sphere AVR-76/20. Likewise, the histogram for the HFR-K3/1 sphere reveals no particles with unusually low ratios. A small amount of the sphere's total cesium inventory (≈0.2%) did show up in the analysis of the matrix graphite and the condensate plates, but this amount is a factor of 50 less than the 10% loss implied by the comparison of the IMGA and KFA pre-heatup data. If there are individual particle failures in sphere HFR-K3/1, this analysis was unable to isolate them from a distribution of nonfailed particles. In contrast to the AVR-76/20 and HFR-K3/1 spheres, the histogram for the HFR-K3/3 sphere is "bimodal," which usually indicates a distribution of failed and nonfailed particles. In this instance, however, it appears that there are two distinct distributions of failed particles and essentially no nonfailed particles. If the ratio of ^{137}Cs to ^{144}Ce reported by KFA in Table 8 (0.0626) is used to represent the ratio of a typical nonfailed particle, we find that the amount of ^{137}Cs retained in the particles after the core heatup simulation test varies from 7% to 93%. The two peaks in the distribution occur at points which correspond to ^{137}Cs retentions of approximately 19% and 57%, respectively. Similar percentages are obtained for the ^{134}Cs isotope.

Figure 8 shows three histograms which illustrate the distribution of ^{154}Eu:^{144}Ce ratios for the three spheres. For the first two spheres, AVR-76/20 and HFR-K3/1, none of the particles exhibit abnormally low ratios to the left of the major distribution. Like the cesium data, this observation contradicts the releases of ^{154}Eu implied by the comparisons with KFA pre-heatup data in Tables 6 and 7. For the HFR-K3/3 sphere, there appears to be a major distribution of particles that have retained their ^{154}Eu as well as 17 particles to the left that have low ^{154}Eu inventories. In all three spheres the average ^{154}Eu value determined by IMGA is approximately 12% lower than the corresponding particle average determined from KFA pre-heatup data. Unfortunately, no ^{154}Eu data was reported in the analysis of the matrix graphite or the condensate plates, so the discrepancy cannot be corroborated. If little or no ^{154}Eu was detected outside the particles, its absence would support the contention that a normalization bias exists between IMGA and KFA pre-heatup data for this isotope as well as for the cesium isotopes.

The final part of the analysis is to provide a statistically significant estimate of the fuel failure fraction for each spherical fuel element. These estimates will be based on cesium retention, since cesium is the most volatile of the isotopes measured and is therefore the best indicator of particle failure. Figure 9 provides a relationship between the number of particles examined, the number of failed particles detected, and the failure fraction at a confidence level of 95%.[5] Based on the analysis of 4940 particles, with no failures being detected, a failure fraction of $\leq 6.0 \times 10^{-4}$ was demonstrated at the 95% confidence level for sphere AVR-76/20. For the HFR-K3/1 sphere, a total of 3514 particles were examined with no failures detected, yielding a failure fraction of $\leq 7.5 \times 10^{-4}$ at the 95% confidence level. In the case of the HFR-K3/3 sphere, almost all of the particles examined showed some loss of cesium, so the failure fraction would be near 1.0.

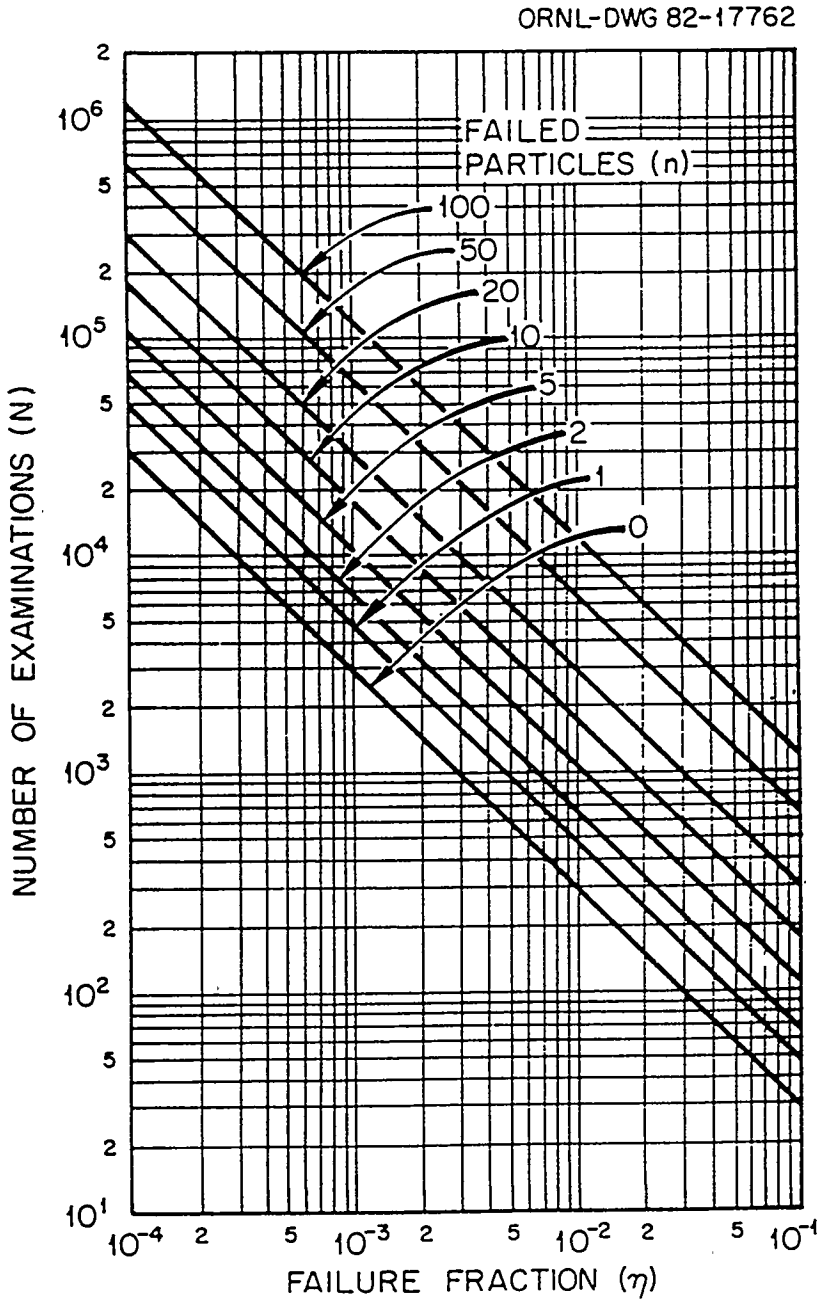

Fig. 9. Number of examinations required to predict failure fractions at the 95% confidence level when various numbers of failed particles are detected during the examination.

6. CONCLUSIONS

Over 10,800 individual LEU UO_2 TRISO-coated fuel particles from three spherical fuel elements were examined by the IMGA system in order to assess fission product behavior at elevated temperatures. Of the three spheres considered, one was reserved as a control and the other two were subjected to simulated accident-condition temperatures of 1600°C and 1800°C, respectively. For the control sphere and the sphere tested at 1600°C, no statistical evidence of fission product release (cesium) from individual particles was observed. In addition, no significant particle-to-particle variation in fission product retention was noted. At fuel temperatures of 1800°C, however, fission product release (cesium) from individual particles was significant, and there was large particle-to-particle variation in retention capabilities. Some of the particles were found to contain only 7% of the expected inventory of cesium, while others contained as much as 93% of the expected inventory. It was also discovered that at 1800°C, individual particle release (cesium) was on average ten times the KFA-measured integral spherical-fuel-element release value. Finally, individual particle-release data from the sphere tested at 1800°C indicate that there may be two distinct modes of failure at fuel temperatures of 1800°C and above.

REFERENCES

1. W. Schenk and H. Nabielek, *Kugelbrennelemente mit TRISO-Partikeln bei Störfalltemperaturen*, Kernforschungsanlage Jülich GmbH, Jül-Spez-487, January 1989.

2. D. C. Kocher, *Radioactive Decay Data Tables*, Technical Information Center, U.S. Department of Energy, DOE/TIC-11026, April 1981.

3. *HBK-Projekt Hochtemperaturreaktor Brennstoffkreislauf Vierteljahresberichte, 3. Quartal 1984*, Kernforschungsanlage Jülich GmbH, 1984.

4. P. E. Brown, A. J. Inns, R. J. Pateman, B. A. Phillips, and B. M. Sharpe, *Post-Irradiation Examination of HTR Fuel Elements*, Harwell Laboratory, Didcot, Oxon, England, AERE-G4740, May 1988.

5. M. J. Kania and H. Nickel, *Performance Assessment of the $(Th,U)O_2$ HTI-Biso Coated Particle Under PNP/HHT Irradiation Conditions*, Kernforshungsanlage Jülich GmbH, Jül-1685, November 1980.

APPENDIX A

DETAILED EXAMINATION RESULTS

Table A.1. IMGA examination summary for clean particles from FRG Set #4 fuels

Step number	Sphere AVR-76/20		Sphere HFR-K3/1		Sphere HFR-K3/3	
	Examination date	Individual particle records	Examination date	Individual particle records	Examination date	Individual particle records
1	30-JAN-89	259	9-JAN-89	56	17-OCT-88	95
2	27-FEB-89	360	15-JAN-89	312	19-OCT-88	212
3	15-FEB-89	392	10-JAN-89	490	14-OCT-88	269
4	2-MAR-89	479	20-JAN-89	280	20-OCT-88	243
5	1-FEB-89	641[a]	13-JAN-89	427	11-OCT-88	149
6	23-FEB-89	605	18-JAN-89	486	13-OCT-88	147
7	6-FEB-89	561	27-OCT-88	330	18-OCT-88	120
8	17-FEB-89	584	29-OCT-88	419	23-OCT-88	344
9	21-FEB-89	528	1-NOV-88	356[a]	21-OCT-88	428
10	8-FEB-89	531	3-NOV-88	358	25-OCT-88	381
Totals		4940		3514		2388

[a] One particle record was eliminated from each of these two steps. Data for these anomalous particles appear separately in tables A.3, A.4, A.18, and A.19.

Table A.2. Parameters used to calculate absolute activities for FRG Set #4 fuels

Isotope	Photon energy (KeV)	Detector efficiency (%)	Branching ratio (%)	Decay constant (s^{-1})	Self-shielding correction factors		
					AVR-76/20	HFR-K3/1	HFR-K3/3
^{106}Ru	511	2.461E-02	2.066E+01	2.179E-08	9.636E-01	9.639E-01	9.643E-01
	622	2.082E-02	9.850E+00		9.718E-01	9.720E-01	9.723E-01
^{134}Cs	604	2.139E-02	9.763E+01	1.065E-08	9.709E-01	9.711E-01	9.714E-01
	795	1.641E-02	8.544E+01		9.788E-01	9.789E-01	9.791E-01
	801	1.629E-02	8.734E+00				9.793E-01
	1364	1.011E-02	3.044E+00			9.867E-01	9.868E-01
^{137}Cs	662	1.958E-02	8.998E+01	7.280E-10	9.738E-01	9.740E-01	9.742E-01
^{144}Ce	133	7.602E-02	1.087E+01	2.822E-08	5.911E-01	5.948E-01	6.001E-01
^{154}Eu	123	7.891E-02	4.052E+01	2.493E-09		5.399E-01	5.454E-01
	723	1.796E-02	1.978E+01			9.765E-01	9.767E-01
	1005	1.339E-02	1.797E+01			9.832E-01	9.833E-01
	1274	1.084E-02	3.551E+01		9.860E-01	9.860E-01	9.861E-01

Table A.3. Mean fission/activation product activities by deconsolidation step for sphere AVR-76/20

Step number	^{106}Ru(622 KeV)		^{134}Cs(604 KeV)		^{137}Cs(662 KeV)		^{144}Ce(133 KeV)		^{154}Eu(1274 KeV)	
	Mean[a]	s(%)	Mean[a]	s(%)	Mean[a]	s(%)	Mean[a]	s(%)	Mean[a]	s(%)
1	1.189E+07	4.43	2.833E+06	2.58	3.799E+06	2.43	4.725E+07	2.61	7.848E+04	7.15
2	1.164E+07	5.16	2.798E+06	2.80	3.769E+06	2.52	4.700E+07	2.65	7.602E+04	6.65
3	1.118E+07	3.90	2.756E+06	2.43	3.723E+06	2.27	4.633E+07	2.35	7.580E+04	6.88
4	1.102E+07	3.53	2.737E+06	2.30	3.708E+06	2.14	4.603E+07	2.39	7.301E+04	7.36
5	1.067E+07	3.56	2.690E+06	2.22	3.666E+06	2.10	4.577E+07	2.43	7.466E+04	7.12
6	1.066E+07	3.64	2.699E+06	2.32	3.660E+06	2.20	4.552E+07	2.32	7.039E+04	7.36
7	1.065E+07	3.61	2.689E+06	2.37	3.676E+06	2.26	4.580E+07	2.48	7.008E+04	7.98
8	1.096E+07	3.76	2.702E+06	2.43	3.682E+06	2.30	4.555E+07	2.47	7.415E+04	7.38
9	1.132E+07	3.88	2.750E+06	2.32	3.726E+06	2.17	4.637E+07	2.49	7.735E+04	6.89
10	1.160E+07	4.21	2.787E+06	2.39	3.764E+06	2.28	4.707E+07	2.37	7.619E+04	7.31
	Corresponding data for the uncharacteristic particle from step 5									
	1.524E+07		3.901E+06		5.349E+06		6.440E+07		1.009E+05	

[a] Bq per particle on October 17, 1985.

Table A.4. Mean fission/activation product activities by deconsolidation step for sphere HFR-K3/1

Step number	^{106}Ru(622 KeV)		^{134}Cs(604 KeV)		^{137}Cs(662 KeV)		^{144}Ce(133 KeV)		^{154}Eu(1274 KeV)	
	Mean[a]	s(%)	Mean[a]	s(%)	Mean[a]	s(%)	Mean[a]	s(%)	Mean[a]	s(%)
1	2.889E+07	4.96	6.562E+06	4.07	5.340E+06	3.81	9.541E+07	4.21	1.891E+05	5.05
2	2.621E+07	7.22	6.343E+06	5.17	5.202E+06	4.62	9.583E+07	5.43	1.822E+05	6.31
3	2.438E+07	6.36	5.950E+06	4.89	4.992E+06	4.50	9.216E+07	5.39	1.657E+05	6.34
4	2.298E+07	6.06	5.699E+06	4.42	4.885E+06	3.98	9.151E+07	5.20	1.569E+05	6.59
5	2.240E+07	7.03	5.380E+06	5.10	4.734E+06	4.55	8.671E+07	5.48	1.511E+05	6.58
6	2.018E+07	6.52	5.088E+06	4.50	4.605E+06	4.01	8.738E+07	4.59	1.402E+05	6.38
7	2.078E+07	6.06	4.942E+06	4.53	4.555E+06	4.04	8.787E+07	4.80	1.380E+05	6.28
8	2.054E+07	5.94	4.827E+06	4.34	4.503E+06	3.90	8.763E+07	4.90	1.372E+05	6.36
9	2.093E+07	6.55	4.747E+06	4.58	4.530E+06	4.24	8.474E+07	4.59	1.366E+05	6.56
10	2.156E+07	6.94	4.760E+06	4.23	4.557E+06	3.90	8.706E+07	4.46	1.393E+05	6.17
	Corresponding data for the uncharacteristic particle from step 9									
	1.840E+07		1.029E+06		1.277E+06		2.029E+07		4.978E+04	

[a] Bq per particle on September 5, 1983.

Table A.5. Mean fission/activation product activities by deconsolidation step for sphere HFR-K3/3

Step number	^{106}Ru(622 KeV)		^{134}Cs(604 KeV)		^{137}Cs(662 KeV)		^{144}Ce(133 KeV)		^{154}Eu(1274 KeV)	
	Mean[a]	s(%)	Mean[a]	s(%)	Mean[a]	s(%)	Mean[a]	s(%)	Mean[a]	s(%)
1	4.120E+07	5.58	3.652E+06	56.71	2.243E+06	57.48	1.207E+08	4.06	2.864E+05	5.56
2	4.136E+07	6.36	3.522E+06	54.98	2.189E+06	55.55	1.212E+08	4.32	2.879E+05	5.40
3	3.834E+07	6.43	4.844E+06	43.10	3.033E+06	43.42	1.172E+08	4.75	2.813E+05	6.14
4	3.619E+07	5.49	5.972E+06	30.50	3.752E+06	30.85	1.161E+08	4.37	2.683E+05	10.08
5	3.598E+07	5.28	6.143E+06	29.76	3.852E+06	30.13	1.131E+08	4.25	2.665E+05	8.35
6	3.462E+07	4.83	6.393E+06	29.72	4.016E+06	30.10	1.127E+08	4.48	2.618E+05	11.63
7	3.589E+07	4.99	6.280E+06	31.22	3.945E+06	31.42	1.156E+08	4.35	2.682E+05	8.96
8	3.676E+07	5.08	5.486E+06	34.59	3.449E+06	34.98	1.147E+08	4.23	2.739E+05	8.41
9	3.804E+07	5.13	4.444E+06	45.16	2.773E+06	45.57	1.158E+08	4.35	2.798E+05	5.77
10	4.064E+07	5.80	3.095E+06	55.45	1.935E+06	55.91	1.198E+08	4.32	2.847E+05	5.64

[a] Bq per particle on September 5, 1983.

Table A.6. ^{106}Ru (622 KeV) : ^{144}Ce (133 KeV) activity ratios for particles from sphere AVR-76/20

Lower[a] Channel Boundary	Number of occurrences by deconsolidation step.										
	Step 1	Step 2	Step 3	Step 4	Step 5	Step 6	Step 7	Step 8	Step 9	Step 10	COMBINED
2.048E-1	0	0	0	0	1	0	0	0	0	0	1
2.078E-1	0	0	0	0	1	2	0	0	0	0	3
2.108E-1	0	0	0	0	4	2	4	0	0	0	10
2.139E-1	0	2	1	1	8	4	5	0	0	0	21
2.169E-1	0	1	0	3	9	10	17	4	1	0	45
2.199E-1	0	0	3	4	37	27	38	7	2	0	117
2.229E-1	0	2	7	13	45	49	47	9	4	2	178
2.259E-1	0	7	21	20	79	61	58	22	13	4	284
2.290E-1	4	5	20	40	106	74	90	44	26	18	428
2.320E-1	8	18	34	56	105	103	97	66	41	26	547
2.350E-1	14	25	52	71	78	82	70	73	42	45	555
2.380E-1	11	30	46	71	65	77	53	84	63	53	555
2.410E-1	15	43	60	57	44	51	46	76	71	64	526
2.441E-1	36	45	53	61	35	30	22	66	74	78	500
2.471E-1	24	36	43	45	16	19	7	54	57	65	368
2.501E-1	28	47	25	20	4	10	1	39	55	61	290
2.531E-1	31	34	10	9	2	3	4	23	33	46	196
2.561E-1	24	20	8	7	2	1	2	8	20	28	121
2.592E-1	28	19	4	1	0	0	0	5	16	18	91
2.622E-1	22	8	3	0	0	0	0	3	4	11	51
2.652E-1	6	6	0	0	0	0	0	1	4	6	23
2.682E-1	3	6	0	0	0	0	0	0	2	4	15
2.712E-1	4	1	1	0	0	0	0	0	0	1	7
2.743E-1	1	3	0	0	0	0	0	0	0	1	5
2.773E-1	0	2	1	0	0	0	0	0	0	0	3

[a] Upper channel boundary for last channel is 2.803E-1.

Table A.7. ^{106}Ru (622 KeV) : ^{144}Ce (133 KeV) activity ratios for particles from sphere HFR-K3/1

Lower[a] Channel Boundary	Number of occurrences by deconsolidation step.										
	Step 1	Step 2	Step 3	Step 4	Step 5	Step 6	Step 7	Step 8	Step 9	Step 10	COMBINED
1.773E-1	0	0	0	0	0	1	0	0	0	0	1
1.837E-1	0	0	0	0	0	1	0	0	0	0	1
1.901E-1	0	0	0	0	0	3	0	0	0	0	3
1.965E-1	0	0	0	0	0	7	0	4	0	1	12
2.029E-1	0	0	0	0	1	15	4	13	0	1	34
2.093E-1	0	0	1	1	2	36	12	21	3	6	82
2.156E-1	0	0	0	4	0	55	29	32	7	7	134
2.220E-1	0	0	3	11	6	81	40	69	19	17	246
2.284E-1	0	2	8	26	25	101	66	69	42	37	376
2.348E-1	0	9	26	27	26	80	64	77	57	55	421
2.412E-1	0	11	33	44	47	46	49	56	50	60	396
2.476E-1	0	17	52	52	72	30	40	47	68	57	435
2.540E-1	0	37	70	37	67	19	14	24	53	44	365
2.604E-1	0	35	79	35	60	7	8	6	27	33	290
2.668E-1	0	43	69	24	43	2	4	0	17	20	222
2.732E-1	1	48	69	8	33	1	0	1	10	14	185
2.795E-1	3	40	36	7	19	1	0	0	1	1	108
2.859E-1	5	28	18	3	10	0	0	0	2	3	69
2.923E-1	13	11	15	0	5	0	0	0	0	1	45
2.987E-1	13	16	8	1	8	0	0	0	0	1	47
3.051E-1	10	6	2	0	3	0	0	0	0	0	21
3.115E-1	5	3	0	0	0	0	0	0	0	0	8
3.179E-1	2	5	1	0	0	0	0	0	0	0	8
3.243E-1	1	1	0	0	0	0	0	0	0	0	2
3.307E-1	3	0	0	0	0	0	0	0	0	0	3

[a] Upper channel boundary for last channel is 3.371E-1.

Table A.8. ^{106}Ru (622 KeV) : ^{144}Ce (133 KeV) activity ratios for particles from sphere HFR-K3/3

Lower[a] Channel Boundary	Number of occurrences by deconsolidation step.										
	Step 1	Step 2	Step 3	Step 4	Step 5	Step 6	Step 7	Step 8	Step 9	Step 10	COMBINED
2.604E-1	0	0	0	1	0	0	0	0	0	0	1
2.650E-1	0	0	0	0	0	0	0	0	0	0	0
2.695E-1	0	0	0	0	0	1	0	0	0	0	1
2.741E-1	0	0	0	1	0	1	0	0	0	0	2
2.786E-1	0	0	0	2	0	1	1	2	0	0	6
2.832E-1	0	0	0	4	1	4	3	1	0	0	13
2.877E-1	0	0	0	11	1	2	5	6	0	0	25
2.923E-1	0	0	2	8	1	11	8	8	2	0	41
2.968E-1	0	0	8	24	8	30	7	11	3	0	91
3.014E-1	0	1	3	30	11	19	17	24	2	4	110
3.059E-1	0	1	13	31	18	22	19	22	12	4	143
3.105E-1	0	2	26	29	20	18	16	35	28	5	179
3.150E-1	4	8	21	29	29	14	14	40	47	15	220
3.196E-1	6	15	34	32	15	13	10	50	54	19	249
3.241E-1	2	14	32	17	17	4	14	51	69	35	255
3.287E-1	15	20	52	10	6	5	4	38	62	44	256
3.332E-1	5	26	27	9	11	0	2	23	62	47	212
3.378E-1	14	23	23	3	5	0	0	19	42	48	176
3.423E-1	21	31	12	2	4	1	0	4	26	48	149
3.469E-1	11	24	6	0	2	0	0	4	13	35	95
3.514E-1	7	21	6	0	0	1	0	5	2	31	73
3.560E-1	5	8	1	0	0	0	0	0	4	28	46
3.605E-1	3	7	1	0	0	0	0	1	0	10	22
3.651E-1	2	8	1	0	0	0	0	0	0	5	16
3.696E-1	0	3	1	0	0	0	0	0	0	3	7

[a] Upper channel boundary for last channel is 3.742E-1.

Table A.9. ^{134}Cs (604 KeV) : ^{144}Ce (133 KeV) activity ratios for particles from sphere AVR-76/20

Lower[a] Channel Boundary	Number of occurrences by deconsolidation step.										
	Step 1	Step 2	Step 3	Step 4	Step 5	Step 6	Step 7	Step 8	Step 9	Step 10	COMBINED
5.467E-2	0	0	0	0	1	0	0	0	0	0	1
5.501E-2	0	0	0	0	0	0	1	0	0	0	1
5.534E-2	0	0	0	0	1	0	0	0	0	0	1
5.568E-2	0	0	0	0	0	1	4	0	0	1	6
5.602E-2	0	0	0	0	4	1	4	2	0	0	11
5.636E-2	0	2	2	3	6	0	9	5	2	1	30
5.669E-2	0	1	2	3	24	5	15	5	9	9	73
5.703E-2	0	6	5	5	21	8	27	11	11	9	103
5.737E-2	1	9	9	10	35	16	32	15	14	16	158
5.771E-2	8	13	14	27	61	19	46	29	29	28	276
5.804E-2	10	17	23	29	63	58	63	43	37	45	388
5.838E-2	15	25	36	34	82	63	78	49	57	63	507
5.872E-2	20	50	44	48	93	82	78	78	58	51	603
5.905E-2	19	43	60	75	67	83	58	82	52	76	619
5.939E-2	36	45	47	63	63	66	47	60	71	66	553
5.973E-2	31	43	38	45	53	67	44	53	63	60	503
6.007E-2	29	27	42	46	22	63	19	50	33	46	375
6.040E-2	35	32	19	35	23	32	18	47	45	24	307
6.074E-2	14	17	13	24	12	17	11	22	22	16	169
6.108E-2	15	17	16	12	6	9	4	17	17	11	120
6.142E-2	9	7	9	11	3	8	2	6	4	3	62
6.175E-2	8	2	10	7	1	4	0	6	3	4	45
6.209E-2	3	3	2	1	0	3	0	4	1	2	19
6.243E-2	3	1	1	1	0	0	1	0	0	0	7
6.277E-2	3	0	0	0	0	0	0	0	0	0	3

[a] Upper channel boundary for last channel is 6.310E-2.

Table A.10. ^{134}Cs (604 KeV) : ^{144}Ce (133 KeV) activity ratios for particles from sphere HFR-K3/1

Lower[a] Channel Boundary	Number of occurrences by deconsolidation step.										
	Step 1	Step 2	Step 3	Step 4	Step 5	Step 6	Step 7	Step 8	Step 9	Step 10	COMBINED
4.896E-2	0	0	0	0	0	0	0	1	0	4	5
5.000E-2	0	0	0	0	0	1	0	10	0	3	14
5.104E-2	0	0	0	0	1	1	2	15	4	23	46
5.208E-2	0	0	0	0	0	2	13	34	17	32	98
5.312E-2	0	0	0	0	0	7	32	68	29	78	214
5.416E-2	0	0	0	0	1	24	53	96	63	81	315
5.520E-2	0	0	0	0	1	45	75	68	90	69	350
5.624E-2	0	1	0	4	6	79	63	68	72	42	335
5.728E-2	0	0	1	6	17	95	40	37	49	14	260
5.832E-2	0	3	7	20	43	83	24	18	20	8	224
5.936E-2	0	2	9	29	44	82	16	3	5	3	194
6.040E-2	0	5	31	44	62	34	8	0	4	0	189
6.144E-2	0	13	53	38	69	15	2	1	1	1	193
6.248E-2	1	27	73	47	60	13	1	0	0	0	221
6.352E-2	1	31	76	49	42	3	1	0	2	0	206
6.456E-2	2	47	73	16	34	2	0	0	0	0	174
6.560E-2	4	52	62	17	18	0	0	0	0	0	153
6.664E-2	8	37	46	6	20	0	0	0	0	0	117
6.768E-2	11	39	28	3	7	0	0	0	0	0	88
6.872E-2	12	23	17	1	2	0	0	0	0	0	55
6.976E-2	8	11	8	0	0	0	0	0	0	0	27
7.080E-2	3	11	4	0	0	0	0	0	0	0	18
7.184E-2	2	5	2	0	0	0	0	0	0	0	9
7.288E-2	0	3	0	0	0	0	0	0	0	0	3
7.392E-2	4	2	0	0	0	0	0	0	0	0	6

[a] Upper channel boundary for last channel is 7.496E-2.

Table A.11. ^{134}Cs (604 KeV) : ^{144}Ce (133 KeV) activity ratios for particles from sphere HFR-K3/3

Lower[a] Channel Boundary	Number of occurrences by deconsolidation step.										
	Step 1	Step 2	Step 3	Step 4	Step 5	Step 6	Step 7	Step 8	Step 9	Step 10	COMBINED
7.685E-3	0	0	0	4	0	4	0	2	0	0	10
1.104E-2	1	2	1	0	2	1	2	1	0	5	15
1.439E-2	13	32	8	2	0	0	1	7	24	110	197
1.775E-2	26	79	54	13	4	3	5	28	97	111	420
2.110E-2	21	31	34	8	7	2	2	28	51	59	243
2.446E-2	11	6	7	2	1	1	4	1	18	18	69
2.781E-2	0	8	4	4	3	2	2	4	8	6	41
3.116E-2	0	2	2	5	2	0	1	7	2	2	23
3.452E-2	1	1	3	3	6	6	2	4	6	0	32
3.787E-2	0	0	5	9	3	4	4	17	10	2	54
4.123E-2	0	0	5	13	7	8	5	21	17	3	79
4.458E-2	0	4	18	22	8	11	9	28	29	9	138
4.793E-2	0	5	20	10	14	5	7	27	27	11	126
5.129E-2	4	9	18	22	9	11	10	30	21	9	143
5.464E-2	3	11	24	28	15	10	9	33	43	10	186
5.800E-2	4	9	21	28	13	11	10	27	29	10	162
6.135E-2	3	4	20	23	13	14	11	31	21	7	147
6.470E-2	5	5	12	17	9	10	11	14	7	1	91
6.806E-2	1	1	10	9	9	9	6	11	9	4	69
7.141E-2	1	1	1	10	7	14	5	8	2	0	49
7.477E-2	1	1	1	6	8	9	7	7	5	2	47
7.812E-2	0	1	0	2	5	8	2	5	1	2	26
8.147E-2	0	0	0	2	0	2	3	2	1	0	10
8.483E-2	0	0	1	1	1	0	1	1	0	0	5
8.818E-2	0	0	0	0	3	2	1	0	0	0	6

[a] Upper channel boundary for last channel is 9.154E-2.

Table A.12. ^{137}Cs (662 KeV) : ^{144}Ce (133 KeV) activity ratios for particles from sphere AVR-76/20

Lower[a] Channel Boundary	Number of occurrences by deconsolidation step.										
	Step 1	Step 2	Step 3	Step 4	Step 5	Step 6	Step 7	Step 8	Step 9	Step 10	COMBINED
7.526E-2	0	0	0	0	1	0	0	0	0	0	1
7.564E-2	0	0	0	0	0	0	0	0	0	0	0
7.602E-2	0	0	1	1	0	1	0	0	0	2	5
7.640E-2	1	2	0	0	4	2	2	2	0	0	13
7.678E-2	1	1	1	3	2	1	6	0	4	4	24
7.717E-2	1	5	2	3	5	5	16	3	8	11	60
7.755E-2	2	12	6	4	15	6	6	6	8	10	73
7.793E-2	6	10	6	7	32	6	15	10	15	26	133
7.831E-2	11	13	20	19	40	17	18	16	25	34	216
7.869E-2	16	22	28	28	37	36	36	18	29	40	291
7.907E-2	26	34	32	30	68	56	41	35	46	44	412
7.945E-2	20	39	41	37	53	66	65	48	43	71	482
7.983E-2	30	46	46	63	81	78	71	61	50	66	592
8.021E-2	34	41	51	58	73	80	55	59	67	58	576
8.059E-2	33	40	36	44	69	61	57	52	51	49	491
8.098E-2	25	32	35	54	61	65	49	66	56	40	482
8.136E-2	13	16	24	35	29	49	48	58	41	33	346
8.174E-2	14	14	21	34	27	26	29	53	35	19	273
8.212E-2	8	15	19	21	19	20	18	29	20	8	176
8.250E-2	10	8	8	16	11	11	16	29	17	7	132
8.288E-2	1	7	4	11	8	8	5	14	5	4	67
8.326E-2	2	1	7	7	5	8	3	11	4	3	51
8.364E-2	3	1	1	1	0	0	2	6	4	2	20
8.402E-2	0	1	3	0	1	1	1	4	0	0	11
8.440E-2	2	0	0	3	0	2	2	4	0	0	13

[a] Upper channel boundary for last channel is 8.479E-2.

Table A.13. ^{137}Cs (662 KeV) : ^{144}Ce (133 KeV) activity ratios for particles from sphere HFR-K3/1

Lower[a] Channel Boundary	Number of occurrences by deconsolidation step.										
	Step 1	Step 2	Step 3	Step 4	Step 5	Step 6	Step 7	Step 8	Step 9	Step 10	COMBINED
4.646E-2	0	0	0	0	0	1	0	6	0	0	7
4.706E-2	0	0	0	0	0	0	0	3	0	0	3
4.766E-2	0	1	1	0	1	3	2	3	0	2	13
4.826E-2	0	3	2	1	1	2	7	12	0	4	32
4.885E-2	0	0	2	2	1	6	12	19	2	3	46
4.945E-2	0	4	2	4	0	9	20	30	2	20	92
5.005E-2	0	5	5	12	7	27	39	61	6	24	186
5.065E-2	0	6	16	20	10	49	40	70	12	29	252
5.125E-2	0	20	35	24	22	57	47	64	34	46	349
5.185E-2	1	20	33	23	23	64	54	40	34	55	343
5.245E-2	3	27	45	36	32	66	32	36	43	59	383
5.305E-2	3	33	53	34	46	53	24	29	59	38	372
5.364E-2	1	35	61	29	50	56	24	25	60	32	373
5.424E-2	5	35	54	29	43	34	10	11	42	23	286
5.484E-2	8	29	47	22	50	33	13	7	26	13	247
5.544E-2	11	24	46	13	35	11	2	1	19	3	166
5.604E-2	5	21	24	17	28	4	1	0	6	5	111
5.664E-2	7	24	21	7	21	8	1	0	5	1	95
5.724E-2	7	9	19	4	19	1	1	2	2	1	64
5.784E-2	0	3	10	2	16	1	1	0	0	0	34
5.843E-2	0	7	7	1	8	1	0	0	2	0	26
5.903E-2	1	4	4	0	5	0	0	0	1	0	15
5.963E-2	1	0	0	0	7	0	0	0	0	0	8
6.023E-2	2	1	2	0	2	0	0	0	1	0	8
6.083E-2	1	1	1	0	0	0	0	0	0	0	3

[a] Upper channel boundary for last channel is 6.143E-2.

Table A.14. ^{137}Cs (662 KeV) : ^{144}Ce (133 KeV) activity ratios for particles from sphere HFR-K3/3

Lower[a] Channel Boundary	Number of occurrences by deconsolidation step.										
	Step 1	Step 2	Step 3	Step 4	Step 5	Step 6	Step 7	Step 8	Step 9	Step 10	COMBINED
4.527E-3	0	0	0	4	0	4	0	2	0	0	10
6.668E-3	1	2	1	0	2	1	2	1	0	4	14
8.809E-3	13	32	8	1	0	0	1	7	22	103	187
1.095E-2	26	78	57	16	4	3	5	25	101	116	431
1.309E-2	22	32	30	5	7	2	1	29	49	61	238
1.523E-2	10	8	8	3	1	1	4	3	19	19	76
1.737E-2	0	7	4	4	3	2	3	4	6	6	39
1.951E-2	0	1	2	5	2	0	1	7	3	2	23
2.166E-2	1	1	4	3	6	7	2	4	8	0	36
2.380E-2	0	0	3	9	4	3	4	17	9	2	51
2.594E-2	0	0	9	17	9	8	5	22	18	3	91
2.808E-2	0	5	18	20	10	10	10	28	35	8	144
3.022E-2	1	5	21	11	9	8	8	28	20	15	126
3.236E-2	5	12	14	21	11	9	8	31	29	7	147
3.450E-2	3	9	30	29	14	11	12	32	43	11	194
3.664E-2	3	8	15	29	16	14	8	29	22	10	154
3.878E-2	2	6	22	25	11	10	12	27	19	5	139
4.092E-2	5	2	12	12	10	10	10	16	9	1	87
4.307E-2	2	1	8	10	6	11	6	9	7	4	63
4.521E-2	1	1	2	8	8	12	4	8	3	0	48
4.735E-2	0	1	0	7	9	9	7	7	5	2	47
4.949E-2	0	1	0	2	3	8	2	5	0	2	23
5.163E-2	0	0	1	1	1	2	3	2	1	0	11
5.377E-2	0	0	0	1	2	1	1	1	0	0	6
5.591E-2	0	0	0	0	1	1	1	0	0	0	3

[a] Upper channel boundary for last channel is 5.805E-2.

Table A.15. ^{154}Eu (1274 KeV) : ^{144}Ce (133 KeV) activity ratios for particles from sphere AVR-76/20

Lower[a] Channel Boundary	Number of occurrences by deconsolidation step.										
	Step 1	Step 2	Step 3	Step 4	Step 5	Step 6	Step 7	Step 8	Step 9	Step 10	COMBINED
1.182E-3	0	0	0	0	0	0	2	0	0	0	2
1.217E-3	0	0	0	0	0	0	3	0	0	0	3
1.252E-3	0	1	0	0	0	6	3	1	0	0	11
1.287E-3	0	0	0	2	2	7	16	6	0	0	33
1.322E-3	0	1	3	8	2	10	11	3	1	1	40
1.356E-3	1	6	0	7	5	30	28	4	3	8	93
1.391E-3	5	7	4	19	19	47	35	11	6	19	172
1.426E-3	6	4	14	27	20	44	65	19	9	18	227
1.461E-3	10	19	20	37	35	59	62	30	11	36	319
1.496E-3	12	29	30	66	52	65	68	44	30	42	441
1.531E-3	21	34	26	49	49	65	63	50	33	58	447
1.566E-3	14	54	64	57	62	67	50	51	56	56	530
1.601E-3	31	53	50	45	76	67	51	77	52	56	557
1.636E-3	36	46	36	47	66	61	41	76	69	53	538
1.670E-3	32	46	36	36	82	35	27	72	63	56	481
1.705E-3	26	22	37	32	62	19	14	51	63	40	364
1.740E-3	24	16	27	25	42	9	8	38	43	47	276
1.775E-3	22	9	20	9	31	8	7	19	25	14	164
1.810E-3	8	8	8	9	20	4	2	11	25	17	112
1.845E-3	5	3	8	4	9	2	1	8	21	4	65
1.880E-3	3	1	7	0	4	0	1	5	13	3	37
1.915E-3	2	0	0	0	0	0	1	4	3	1	12
1.950E-3	1	1	2	0	1	0	2	4	1	1	12
1.984E-3	0	0	0	0	1	0	0	0	0	1	2
2.019E-3	0	0	0	0	1	0	0	0	1	0	2

[a] Upper channel boundary for last channel is 2.054E-3.

Table A.16. ^{154}Eu (1274 KeV) : ^{144}Ce (133 KeV) activity ratios for particles from sphere HFR-K3/1

Lower[a] Channel Boundary	Number of occurrences by deconsolidation step.										
	Step 1	Step 2	Step 3	Step 4	Step 5	Step 6	Step 7	Step 8	Step 9	Step 10	COMBINED
1.318E-3	0	0	0	0	0	3	2	5	0	1	11
1.356E-3	0	0	0	0	0	1	7	4	2	2	16
1.394E-3	0	0	0	0	0	11	11	16	3	11	52
1.432E-3	0	0	0	2	1	14	18	36	11	14	96
1.469E-3	0	0	0	1	2	46	39	49	23	22	182
1.507E-3	0	0	0	8	8	57	45	57	50	49	274
1.545E-3	0	1	4	11	16	73	57	73	46	47	328
1.583E-3	0	1	16	22	30	83	60	66	57	66	399
1.621E-3	0	0	20	34	47	67	41	51	58	46	366
1.659E-3	0	5	39	51	35	46	24	29	40	50	319
1.696E-3	0	5	56	34	58	30	14	19	31	29	276
1.734E-3	1	19	64	36	57	35	7	8	21	11	258
1.772E-3	0	18	70	31	55	12	3	5	11	6	212
1.810E-3	2	37	65	25	39	4	1	1	1	2	177
1.848E-3	3	54	54	14	37	1	1	0	2	0	166
1.886E-3	11	45	43	7	23	2	0	0	0	1	132
1.923E-3	9	45	28	3	13	0	0	0	0	0	98
1.961E-3	9	29	16	1	3	1	0	0	0	1	60
1.999E-3	5	25	7	0	2	0	0	0	0	0	39
2.037E-3	5	9	3	0	0	0	0	0	0	0	17
2.075E-3	3	10	4	0	1	0	0	0	0	0	18
2.113E-3	3	4	0	0	0	0	0	0	0	0	7
2.150E-3	5	4	1	0	0	0	0	0	0	0	10
2.188E-3	0	0	0	0	0	0	0	0	0	0	0
2.226E-3	0	1	0	0	0	0	0	0	0	0	1

[a] Upper channel boundary for last channel is 2.264E-3.

Table A.17. ^{154}Eu (1274 KeV) : ^{144}Ce (133 KeV) activity ratios for particles from sphere HFR-K3/3

Lower[a] Channel Boundary	Number of occurrences by deconsolidation step.										
	Step 1	Step 2	Step 3	Step 4	Step 5	Step 6	Step 7	Step 8	Step 9	Step 10	COMBINED
4.831E-4	0	0	0	1	0	0	0	1	0	0	2
5.724E-4	0	0	0	0	0	1	0	0	0	0	1
6.618E-4	0	0	0	0	0	0	0	0	0	0	0
7.511E-4	0	0	0	2	0	0	0	0	0	0	2
8.405E-4	0	0	0	0	0	1	0	1	0	0	2
9.298E-4	0	0	0	1	0	1	2	1	0	0	5
1.019E-3	0	0	0	0	0	1	0	0	0	0	1
1.108E-3	0	0	0	0	2	0	0	1	0	0	3
1.198E-3	0	0	0	0	0	1	0	0	0	0	1
1.287E-3	0	0	0	0	0	0	0	0	0	0	0
1.377E-3	0	0	0	0	0	0	0	0	0	0	0
1.466E-3	0	0	0	0	0	0	0	0	0	0	0
1.555E-3	0	0	0	0	0	0	0	0	0	0	0
1.645E-3	0	0	0	0	0	0	0	0	0	0	0
1.734E-3	0	0	0	0	0	0	0	0	0	0	0
1.823E-3	0	0	0	0	0	0	0	0	0	0	0
1.913E-3	0	0	0	2	0	0	0	0	1	0	3
2.002E-3	0	0	0	3	4	0	0	2	2	0	11
2.091E-3	2	1	4	8	2	4	4	3	5	11	44
2.181E-3	11	29	23	36	20	17	23	23	21	48	249
2.270E-3	29	67	62	77	31	41	37	78	87	111	619
2.359E-3	34	68	104	86	50	48	38	115	150	112	807
2.449E-3	16	41	56	25	34	23	13	80	116	82	487
2.538E-3	3	6	17	2	6	9	3	30	36	15	127
2.627E-3	0	0	3	0	0	0	0	9	10	2	24

[a] Upper channel boundary for last channel is 2.717E-3.

Table A.18. Summary of mean activity ratios by deconsolidation step for sphere AVR-76/20

Step number	^{106}Ru:Ce ratio		^{134}Cs:Ce ratio		^{137}Cs:Ce ratio		^{154}Eu:Ce ratio	
	Mean	s(%)	Mean	s(%)	Mean	s(%)	Mean	s(%)
1	2.516E-01	3.75	5.998E-02	1.83	8.042E-02	1.64	1.661E-03	6.71
2	2.476E-01	4.14	5.953E-02	1.79	8.021E-02	1.67	1.618E-03	6.30
3	2.414E-01	3.56	5.949E-02	1.83	8.038E-02	1.66	1.636E-03	6.85
4	2.394E-01	3.27	5.946E-02	1.80	8.057E-02	1.66	1.586E-03	7.09
5	2.331E-01	3.33	5.879E-02	1.79	8.012E-02	1.65	1.632E-03	7.08
6	2.342E-01	3.34	5.930E-02	1.67	8.041E-02	1.54	1.546E-03	7.27
7	2.327E-01	3.32	5.872E-02	1.83	8.028E-02	1.71	1.530E-03	7.79
8	2.406E-01	3.45	5.933E-02	1.84	8.084E-02	1.71	1.628E-03	7.23
9	2.441E-01	3.61	5.931E-02	1.80	8.038E-02	1.68	1.669E-03	6.82
10	2.464E-01	3.58	5.922E-02	1.72	7.998E-02	1.61	1.619E-03	7.14
COMBINED[a]	2.400E-01	4.27	5.925E-02	1.87	8.036E-02	1.68	1.608E-03	7.59
	Corresponding data for the uncharacteristic particle from step 5							
	2.366E-01		6.057E-02		8.305E-02		1.566E-03	

[a] Data in this row represents a combination of data from all 10 steps.

Table A.19. Summary of mean activity ratios by deconsolidation step for sphere HFR-K3/1

Step number	^{106}Ru:Ce ratio		^{134}Cs:Ce ratio		^{137}Cs:Ce ratio		^{154}Eu:Ce ratio	
	Mean	s(%)	Mean	s(%)	Mean	s(%)	Mean	s(%)
1	3.029E-01	4.19	6.883E-02	3.55	5.601E-02	3.45	1.984E-03	4.91
2	2.738E-01	6.54	6.626E-02	4.27	5.435E-02	4.05	1.903E-03	5.48
3	2.649E-01	6.13	6.463E-02	3.94	5.424E-02	3.85	1.800E-03	5.79
4	2.514E-01	5.94	6.235E-02	3.79	5.345E-02	3.63	1.715E-03	5.59
5	2.587E-01	6.56	6.212E-02	4.34	5.467E-02	4.03	1.744E-03	6.17
6	2.312E-01	6.20	5.828E-02	3.67	5.274E-02	3.30	1.605E-03	6.01
7	2.367E-01	5.35	5.629E-02	3.62	5.188E-02	3.25	1.572E-03	5.65
8	2.347E-01	5.76	5.513E-02	3.56	5.144E-02	3.30	1.567E-03	5.71
9	2.471E-01	5.59	5.605E-02	3.32	5.349E-02	2.97	1.612E-03	5.52
10	2.477E-01	6.33	5.471E-02	3.38	5.238E-02	3.10	1.601E-03	5.73
COMBINED[a]	2.500E-01	8.58	5.968E-02	7.99	5.324E-02	4.13	1.683E-03	8.89
Corresponding data for the uncharacteristic particle from step 9								
	9.064E-01		5.072E-02		6.292E-02		2.453E-03	

[a] Data in this row represents a combination of data from all 10 steps.

Table A.20. Summary of mean activity ratios by deconsolidation step for sphere HFR-K3/3

Step number	^{106}Ru:Ce ratio		^{134}Cs:Ce ratio		^{137}Cs:Ce ratio		^{154}Eu:Ce ratio	
	Mean	s(%)	Mean	s(%)	Mean	s(%)	Mean	s(%)
1	3.414E-01	3.43	3.053E-02	58.68	1.875E-02	59.45	2.373E-03	3.89
2	3.410E-01	3.91	2.932E-02	57.06	1.823E-02	57.64	2.375E-03	3.66
3	3.270E-01	4.02	4.167E-02	44.37	2.610E-02	44.68	2.399E-03	4.07
4	3.118E-01	4.27	5.171E-02	31.29	3.249E-02	31.64	2.315E-03	9.83
5	3.183E-01	3.87	5.464E-02	30.92	3.426E-02	31.28	2.358E-03	7.55
6	3.075E-01	3.97	5.707E-02	30.44	3.585E-02	30.81	2.330E-03	11.94
7	3.106E-01	3.87	5.457E-02	31.65	3.428E-02	31.84	2.322E-03	8.52
8	3.208E-01	4.25	4.816E-02	35.67	3.028E-02	36.05	2.392E-03	8.18
9	3.285E-01	3.36	3.872E-02	46.79	2.416E-02	47.20	2.416E-03	4.25
10	3.393E-01	3.94	2.602E-02	57.29	1.627E-02	57.77	2.377E-03	4.34
COMBINED[a]	3.261E-01	5.14	4.147E-02	48.15	2.597E-02	48.62	2.375E-03	6.81

[a] Data in this row represents a combination of data from all 10 steps.

DOE-HTGR-88381
ORNL/TM-11455
Distribution
Category UC-522

INTERNAL DISTRIBUTION

1-2. Central Research Library
3. Document Reference Section
4-5. Laboratory Records Department
6. Laboratory Records, ORNL RC
7. ORNL Patent Section
8-10. M&C Records Office
11-20. C. A. Baldwin
21. W. P. Barthold (Consultant)
22. E. E. Bloom
23. J. A. Bucholz
24. T. D. Burchell
25. W. P. Eatherly (Consultant)
26. L. C. Emerson
27. W. A. Gabbard
28. R. K. Genung
29. J. R. Hightower
30. F. J. Homan
31. D. T. Ingersoll
32. H. Jones
33-42. M. J. Kania
43. P. R. Kasten (Consultant)
44. J. C. Mailen
45. D. L. Moses
46. B. F. Myers
47. N. H. Packan
48. P. L. Rittenhouse
49. O. M. Stansfield
50. J. O. Stiegler
51. D. B. Trauger
52. A. W. Trivelpiece
53. B. A. Worley
54. J. R. Weir, Jr.
55. J. C. Whitson
56. A. Zucker

EXTERNAL DISTRIBUTION

57-59. GENERAL ATOMICS, P.O. Box 85608, San Diego, CA 92138-5608

G. C. Bramblett
A. J. Neylan
R. F. Turner

60. KERNFORSCHUNGSANLAGE JÜLICH GmbH, Postfach 1913, D-5170, Jülich, Federal Republic of Germany

H. Nabielek

61-62. MODULAR HTGR PLANT DESIGN CONTROL OFFICE, P.O. Box 85608, San Diego, CA 92138-5608

R. R. Mills
J. P. Sanders

63-65. DOE, DIVISION OF HTGRs, NE-451, Washington, DC 20545

J. E. Fox
M. E. Long
E. Purvis

66. DOE, OFFICE OF ADVANCED REACTOR PROGRAMS, NE-45, Washington, DC 20545

    Director

67. DOE, SAN, 1333 Broadway, Oakland, CA 94612

    S. El-Safwany

68. DOE, OAK RIDGE OPERATIONS OFFICE, Office of Assistant Manager for Energy Research and Development, P.O. Box 2001, Oak Ridge, TN 37831-8600

    L. K. Fletcher

69-123. DOE, OFFICE OF SCIENTIFIC AND TECHNICAL INFORMATION, Office of Information Services, P.O. Box 62, Oak Ridge, TN 37831

    For distribution as shown in OSTI-4500, Distribution Category UC-522 (Gas-Cooled Reactor Technology)